GNEC 153
REACTOR TECHNOLOGY

ANALYSIS OF THE INITIAL NUCLEAR SUPERHEAT CRITICAL EXPERIMENTS

Supplementary Study
Related to BONUS And Nuclear Superheat Programs

Prepared Under Contract With The
UNITED STATES ATOMIC ENERGY COMMISSION
AEC Contract AT(40-1)-2674

January 30, 1961

GENERAL NUCLEAR ENGINEERING CORPORATION
Dunedin, Florida

DISCLAIMER

ABSTRACT

The initial measurements in the Nuclear Superheat (NUSU) Critical Experimental program were performed for the purpose of investigating core arrangements of solid-rod boiler and superheater fuel similar to those used in the Boiling Nuclear Superheater (BONUS) project. In these experiments, the boiler region contained aluminum-clad fuel rods of 1.85 wt.% U^{235} enrichment and some rods of natural enrichment. The superheater region was composed of rod-in-tube elements, the fuel rod having 3.41 wt.% U^{235} enrichment and a stainless-steel clad. The experimental procedures involved a determining of criticality by the adjustment of water height and the measuring of power distributions by the direct measurement of fuel-rod activity.

In conjunction with the experimental program, a detailed analytical program was initiated for the purpose of planning and interpreting the experiments as well as of evaluating and developing analytical methods. The basic method of analysis that was employed was described in detail in a previous report[1]. In addition, a simple theory was developed to interpret partial water-height critical measurements; the theory permits direct evaluation of the accuracy of the analytical methods at the time the experiment is performed, and enables detailed calculations to be carried out in advance of the experiments.

For those experiments that were analyzed, the reactivity and rod-by-rod power distributions were calculated. The interpretation of the experiments has yielded information concerning:

1) The effect of different boiler-superheater geometrical arrangements;
2) the reactivity changes associated with the voiding and flooding of the superheater region;
3) the power regulation between boiler and superheater regions;
4) the determination of epithermal transmission probabilities for cadmium and boron-stainless-steel rods;
5) the power flattening of individual boiler assemblies by arrangement of fuel, moderator, and neutron poison;

6) the void simulation by the insertion of aluminum rods as a function of position within the boiler fuel assembly.

The calculational methods used in the analyses of the initial NUSU Critical Experiments predict the measured reactivity and power distributions to within the limits of uncertainty of the experimental techniques, which include the uncertainties in core dimensions and compositions. For the boiler fuel arrangements, the calculated reactivities agree to within 1.5 per cent Δk, and the individual fuel-rod power distributions are in very good agreement with the measurements. For the boiler-superheater fuel arrangements, the reactivity predictions are in better agreement, within 1.0 per cent Δk, but the power distributions indicate that the reactivity of the superheater relative to the boiler is somewhat less than calculated.

Table of Contents

List of Tables

List of Illustrations

I. INTRODUCTION

A. The Initial Nuclear Superheat (NUSU) Experimental and Analytical Program

On July 1, 1959, Combustion Engineering, Inc. contracted (Contract No. AT(11-1)-795) with the U.S. Atomic Energy Commission to conduct a development program on a boiling-water reactor incorporating nuclear superheat. Part of this program included the performance of critical experiments that would carefully examine the nuclear problems associated with an integral nuclear superheat reactor.[2] For the first phase of the experimental program, a solid-rod superheater element was investigated, since this type of element represents a fuel element that could be fabricated with established manufacturing techniques.

Prior to the NUSU contract, extensive analytical studies had already been completed for the Boiling Nuclear Superheater (BONUS) reactor which contained solid-rod elements in both the boiler and superheater regions.[3,4] The BONUS reactor design involved nuclear concepts that were quite different from previous light-water designs, and definitely required the performance of critical experiments for the purpose of verifying the analysis. Therefore, it was decided to combine the objectives of both projects, NUSU and BONUS, for the initial critical experiments and to use approximately the same rod size, enrichment, and water-to-fuel ratio for both the boiler and superheater regions as was used for the BONUS core. In this manner, the same fuel could later be used for the detailed BONUS Mockup Experiment;* and, as a result, a substantial reduction of the cost of the total reactor critical experimental program would be achieved.

In conjunction with the initial experimental program, a detailed analytical program was initiated. The experimental program was planned

---

* The BONUS Critical Program will utilize critical assemblies of full BONUS size. This program is part of the BONUS project Research and Development Program and is being performed by Combustion Engineering Inc., Windsor, Connecticut. The experiment began in January 1961.

so that it would be readily susceptible to analysis. These experiments were only concerned with "engineering"-type measurements; i.e., criticality, power distribution, and differential reactivity-change measurements. Criticality was obtained by critical water height; power distribution was determined by fuel-element activation; differential reactivity measurement was made by the variation of critical water height. With the experimental program established in terms of such measurements, a considerable number of detailed calculations could be performed in advance of the measurements, and the analytical methods could be evaluated at the time the measurements were performed. This procedure gave more credence to the analysis, and allowed during the experiments a rapid shift in the experimental program to areas that required more exploration, thus expanding the range of the program.

B. The Role of Cold Critical Experiments in Power Reactor Design

Although the critical experiment is a powerful tool for the neutron-physics design of power reactors, and one which, in principle, can be used to check the neutron-physics behavior to a high degree of precision, practical considerations often impose important limits on its range of usefulness and on its precision. The straightforward method of applying the critical is as a "nuclear mockup" of the actual reactor, and it is in this sense that one can obtain almost any degree of precision of results if one is willing to spend the effort necessary to achieve a corresponding degree of precision of mockup. The usual practical limitations are the expense and difficulty of duplicating operating conditions, reactor design tolerances, and, in some cases, reactor materials and full reactor sizes. An additional practical difficulty is that critical experiments usually must be made before the reactor design is frozen. These practical limitations are particularly severe for H_2O-moderated power reactors because the short thermal-neutron diffusion length in H_2O-moderated lattices requires great precision of detail for a good nuclear mockup, and because the neutron-physics properties of the lattice change so greatly between room temperature

and reactor operating temperature; in a boiling water reactor a further difficulty of the latter type enters because of the presence of steam voids in the operating reactor. It is probably safe to say that no good nuclear mockup of an operating H_2O power reactor can be made except in a high-temperature (pressurized) critical facility.

When it is clear that a good nuclear mockup is not practical, the reactor physicist may resort to one of two remaining alternative approaches to a critical program. He may settle for some approximation to a nuclear mockup, in which, for example, he may attempt to simulate changes in water density by changes in lattice spacing, or by the use of low-cross-section materials as water displacers; or he may reject the idea of a mockup completely, and use the critical assembly simply as a means of checking his calculational techniques. In the former case the theoretical operations necessary to correct the experimental results for the imperfect simulation may sometimes be more difficult, or more uncertain, than the calculation of the reactor itself; or the complications introduced by simulation attempts may result in an experiment that poses more theoretical problems than the reactor itself. In the latter case the critical assembly, while not a mockup or simulation of the actual reactor, must resemble it in those respects that will pose adequate tests for the calculation procedures.

In the work treated here the choice of alternatives was straightforward, for the time allotted to experiments directed toward the BONUS design was short, and the experiments constituted only a preliminary investigation of that configuration; at the same time results of some generality were desired. The experiments were made primarily to check the accuracy of the calculation methods for configurations typical of, but not identical with, the BONUS reactor. Lattices were investigated which approximated the fuel-element configurations, fuel enrichments, fuel/water ratios, and degree of fuel-element clustering of the BONUS boiling region, as were also composite assemblies approximating portions of the BONUS boiler section in combination with a superheater section. However, certain less significant features of the BONUS lattice, such as the zirconium fuel-assembly boxes, were

omitted; and the boiler-superheater assemblies utilized only a single slab of superheater elements, adjacent to the boiler, whereas the BONUS reactor comprises four such superheater slabs, around the central, square, boiler region.

It is the purpose of this report to present a comparison of the experimental results with the results of the calculations of the experimental configurations, made before the experiments were performed. This aspect of the critical program constitutes a test of the calculational methods used in the BONUS reactor design.

C Nuclear Problems Introduced by Integral Nuclear Superheat

A boiling-water reactor with integral nuclear superheat behaves as though it were two reactors that are nuclearly coupled. Saturated steam that has been created from the water upon passage through the boiler region, is raised to superheat temperatures upon passage through the superheat region. The following nuclear problems are associated with the core design:

1) Safety. Since, upon startup, the steam coolant channels will usually contain water, it is necessary to design the reactor such that the reactivity change associated with the removal of water is below a preassigned value at reactor startup. Also, the reactivity associated with accidental flooding of the superheater under operating conditions should not be permitted to exceed a specified value.
2) Control System. The boiler produces a specific amount of steam that is raised to appropriate superheat temperatures in the superheater. It is required that an adequate control system, which includes the size, number, and position of control elements be used to regulate the power output of each region under both steady-state and transient conditions.
3) Local Power Peaking. Since the core arrangement will necessarily involve two different types of elements with

different water-to-fuel ratios, local distorting of the fluxes can occur which give rise to local peaking factors that may be larger than desired.

4) Fuel Burnup. The reactivity change with fuel burnup could be quite different for the boiler and superheater region, which increases the difficulty of maintaining the proper division of power between the two regions. Also, a dissimilarity of the specific power in the two regions could require different fuel cycles with the associated problems of maintaining the proper split in power without producing power distortions.

5) Reactor Stability. The usual problems associated with the stability of a boiling-water reactor are also present in a boiling-water reactor with integral nuclear superheat. In addition, there will be some boiling in the superheater due to gamma rays and heat leakage which will contribute to the boiling void coefficient of the reactor.

Most of these problems are associated with the hot operating conditions of the reactor, and cannot be solved directly by a cold clean critical experiment. Also, the particular fuel elements that are used for these initial NUSU critical experiments may not represent the types that will ultimately be most attractive for superheater reactors. Nevertheless, these experiments, which involved a large number of geometric arrangements, will indicate the range of validity of analytical methods which, in turn, can then be applied to the operating design considerations.

II. METHOD OF ANALYSIS

A three-group method of analysis, which has been developed for the purpose of analyzing light-water UO_2 cores of low enrichment, has been used to analyze these experiments. A complete description of the method, together with the analysis of previous critical experiments, is presented in another report.[1] Briefly, the method entails the consolidation of a series of subroutines to produce a set of self-consistent multigroup parameters. The thermal cross sections are determined by averaging the cross section over a "hardened" or shifted Maxwellian spectrum, the amount of hardening being a function of the macroscopic absorption-to-slowing-down ratio. The disadvantage factor for a solid-rod fuel element is calculated using diffusion theory for the moderator and a transport condition at the surface of the rod, the accuracy of the calculation for this case being comparable to a P-3 calculation. The epithermal capture cross section of U^{238} is based on the measurement of Hellstrand including a 1.1 barn $\frac{1}{v}$ absorption, and ignores epithermal self-shielding effects even for very close-packed lattices. The fast-fission factor is calculated relative to the experimental measurements for UO_2 lattices. The diffusion coefficients are found by averaging the measured cross sections over the appropriate neutron flux in each neutron energy group. The slowing-down cross section is defined as the diffusion coefficient divided by the neutron age, the age being determined by calculating equivalent transport and slowing-down factors relative to light-water measurements. A correction which increases the absorption cross section of the water channels within the core is applied to account for the discontinuity in neutron temperature between the fuel region and water channel regions. The fuel region is divided into unit cells such that a specified amount of water is assigned to a fuel rod. All water in excess of this amount is defined as a channel region. The three-group constants are computed for each region in the core. For complex geometries, the three-group equations are solved by the

IBM-704 PDQ two-dimensional code.[5] The resulting power distribution in the fuel region is averaged over each of the unit cells, and rod-by-rod power distributions are generated.

This entire analytical "package," using a simple theoretical model with the best basic measurements for nuclear data, has been able to predict the nuclear characteristics of cold critical experiments with a high degree of precision. The relatively simple recipes used in this method permits the analyst to exercise control of the calculation at its inception, through machine processing, and, finally, through an interpretation of the results. Often the initial calculation can be approximated or the machine calculation results can be used to generate parameters that permit accurate hand calculations. Any errors, human or machine, are easily located. Thus, the over-all method tends to be precise, fast, and economical.

This method was developed almost entirely before the performance of UO_2-fueled critical experiments. When critical experimental information became available, the comparison between theory and experiment revealed very close agreement with entirely minor modifications in the averaging procedures. Therefore, there has been little effort to evaluate the effect of changing the various parameters involved in the method. Undoubtedly, a combination of alternative procedures would yield equally satisfactory results. However, since this method works for engineering design and, as a matter of fact, works well, there is very little incentive to change it.

From the theoretical point-of-view, a large number of objections can be leveled at the entire analytical procedure. However, these objections would not be valid criticisms, since it is claimed that this method only correlates experimental results with reasonably good accuracy. Other fields of engineering utilize gross experimental measurement to derive empirical expressions to guide the analysis. Perhaps, because the physical laws and mathematical equations are better known, a reactor core calculation is usually not considered valid unless it goes back to first principles. However, it should be noted that the so-called "rigorous" and "exact" theoretical

formulations necessarily degenerate into approximate solutions when faced with the uncertainties in nuclear data and the geometrical complexities found in ordinary engineering core designs.

Although there is agreement between theory and cold critical experiments, it remains to be seen how well the agreement is maintained for the hot operating condition of the reactor. For the BONUS project post-construction research and development program, it is proposed that detailed measurements be made on the reactor core to evaluate these methods under operating conditions. At present, the prime ingredients of the initial (low plutonium concentration) hot operating conditions have been investigated by the cold experiment. By varying the geometrical complexity of the core, the water-to-fuel ratio, and the fuel enrichment, the hot condition can be simulated. Therefore, if there is agreement for all these conditions, there is a high probability that the accuracy will sustain itself under hot conditions. In fact, critical experiments using highly-enriched fuel show that the accuracy is maintained at elevated temperatures.[6] The inclusion of large concentrations of plutonium probably can be handled by using effective thermal cross sections for the different plutonium isotopes. These effective cross sections would be based on the combination of cross-section data and reactivity measurement under power reactor conditions.

A. Application to Reactor Design

The NUSU critical experiments have introduced additional factors that require an extension of the analytic methods and procedures described in reference 1. These factors concern the definition of the minimum size of a fuel region, the method of calculating the fast-fission factor for a multizone core, calculations of the disadvantage factors for the superheater element and for boron-pyrex annular rods, control-rod analysis, neutron streaming along the voided superheater element, and determination of rod-by-rod power distribution from the problem output of the PDQ code.

1. Minimum-Size Fuel Region

A core region is defined as either being a diffusion or control-rod region. For a diffusion region, with the exception of the fast-effect calculation, the three-group diffusion theory constants are calculated independently of the surrounding regions. For a control-rod region, a transport condition is applied at the boundary of the region for those neutron energy groups that require it -- usually the thermal and epithermal groups. A structural region such as aluminum or stainless steel can also be treated as an independent region, but its thermal cross sections are based on the neutron temperature of the adjacent region, usually a water channel. In the definition of a region, no minimum size has been specified. It appears that if it is valid to apply diffusion theory within a region, then linking these regions with the usual diffusion theory continuity conditions yields answers that are in good agreement with experiment. Normally, a fuel region is composed of several identical unit cells such that diffusion theory should apply to the over-all dimensions. However, if different types of fuel elements, or possibly a neutron poison, are inserted into the fuel region, it would be desirable to treat these inhomogenieties discretely rather than by averaging their affect over the entire fuel region.

In the NUSU experiments, several configurations were analyzed in which small core areas are treated as separate regions. For the 32-rod fuel assembly, two different configurations involving the same amount of aluminum were analyzed. One arrangement had 16-1/4-inch rods positioned interstitially between fuel rods, the other had 4-1/2-inch rods in the center of the assembly. If the analysis were carried out assuming a uniform distribution of aluminum and water channel within the fuel region, both of these assemblies, which contain the same total amount of aluminum and water, would yield the same reactivity. However, treating the region discretely with the aluminum associated either with a fuel region or with a water channel region, predicts a different reactivity which agrees with the measurement. Two other

experimental measurements involved inserting natural-uranium rods and a few borated poison rods at the corners of 1.85 wt.% U^{235}-enriched assemblies. For these cases, the fast fission factor remains essentially unchanged. Both of these experiments were analyzed assuming the 0.625 x 0.625 sq in. corner areas as separate regions. It will be noted that the agreement with experiments is quite good. Thus, it appears possible to use these methods for analyzing heterogeneous closely packed lattices.

2. The Fast-Fission Factor

Presently, the fast-fission factor is calculated relative to an experimental measurement. For this calculation, the entire region is treated as if it were homogeneous, since the measurements have shown that, for small rods and closely packed lattices, the fast-fission factor is mainly dependent on water-to-uranium atom ratio.[7] This method of calculation is sufficiently accurate for most purposes and is very convenient for the performance of hand calculations. However, when a core possesses a multizone fuel loading, an arbitrariness arises in associating the water channels and structural materials that exist between fuel regions with the respective fuel regions. Also, for a unit cell analysis, it would be desirable to include the effect of a fast fission over a small area. For these reasons, an alternate method for calculating the fast-fission factor has been developed in which a first-group absorption and fission cross section are determined for U^{238}.

Using the Yankee,[8] N.S. Savannah[9] and the NUSU critical experiments, the following average first-group microscopic cross sections were determined for U^{238}:

$$\sigma_a = 0.275 \times 10^{-24} \text{ cm}^2$$

$$\nu\sigma_f = 0.605 \times 10^{-24} \text{ cm}^2$$

where the subscripts a and f refer to the absorption and the fission cross sections, respectively; and ν is the number of prompt neutrons created during the fission process.

For the analysis of the NUSU experiment, the homogeneous method of determining the fast-fission factor has been used. In calculating the total area for the fast-fission factor calculations, it has been assumed that materials between fuel regions are equally divided between these regions.

3. Disadvantage Factor

For solid-rod elements, the analytic expression, described in reference 1, duplicated P-3 thermal utilization calculations. This expression calculates ϕ_m/ϕ_f, which is the disadvantage factor of the moderator relative to the fuel. The disadvantage factor applied to the clad is $\frac{1 + \frac{\phi_m}{\phi_f}}{2}$. For the calculation of disadvantage factors for the superheater element including the surrounding coolant tube, the analytical method has been used. The assumptions are made that for the coolant tube voided, the coolant tube has the same disadvantage factor as clad; for the coolant tube flooded, the coolant tube has the same disadvantage factor as the water. These assumptions were later checked with P-3 calculations, and there is good agreement in the prediction of thermal utilization for this element.

The borated rods (Table IV) consist of annular borated pyrex regions with internal water regions. A P-3 calculation[10] was performed to obtain the disadvantage factor for these rods. The input data for the P-3 calculation use cross sections that are hardened in the same manner as any region within the core. For hydrogen, the average isotropic scattering cross section, σ_o, and the first-order correction for anisotropic scattering, σ_1, used in the P-3 calculations are given in Figure 1.

4. Control-Rod Analysis

A control-rod region is defined as one in which the thermal neutron absorption cross section is greater than the scattering cross

section. For such a region a transport condition is applied at the surface of the rod which is related to the probability of a neutron penetrating the region. The assumption is made that it is only necessary to consider the rod absorptions in the thermal and epithermal group, the fast-group constants being determined in the same manner as for a diffusion region.

The quantity, d (the reciprocal of the logarithmic derivative of the flux at the surface of an absorber), can be related to the transmission probability of a neutron penetrating a slab. From simple diffusion theory, for a slab in an infinite medium,

$$d = \frac{2}{3} \lambda_t \frac{(1 + T)}{(1 - T)} \qquad (1)$$

where λ_t is the transport mean free path, and T is the transmission probability. For a black absorber, T = 0, and $d = \frac{2}{3} \lambda_t$. For a rod region, a parameter, C, can be defined as follows:

$$C = \frac{D \Delta \phi}{\phi} = \frac{1}{2} \frac{D}{d} = \frac{1}{2} \frac{(1 - T)}{(1 + T)} \qquad (2)$$

Such a parameter is incorporated into the PDQ code[5] to define a rod region. The parameter, C, is determined analytically for the thermal group and experimentally for the epithermal group. For the thermal group, the scattering cross section is neglected, and only the absorption is considered. The transmission probability can be approximated by the following expression:[11]

$$T_3 = 2 E_3 (\Sigma t)$$

where:

$$E_3 (\alpha) = \int_1^\infty \frac{\exp (- \alpha x)}{x^3} d x \qquad (3)$$

t = the thickness of the control slab

Σ = the average macroscopic absorption cross section

The average macroscopic absorption cross section of the rod is based on the neutron temperature of the water channel region.

The value of the epithermal transmission probability, T_2, can be found directly from critical experiments by determining the value of T_2 that permits a core with control rods to have the same absolute reactivity as a core without rods. Such measurements boiler fuel assemblies, and the values of T_2 were determined for two different thicknesses of cadmium and borated stainless-steel slabs. These values were then used in analysis of the boiler-superheater core arrangements.

5. Neutron Streaming Along Superheater Tubes

Voiding of the superheater tubes permits neutrons to stream vertically along the tubes. The resulting leakage of neutrons from the core will be underestimated if the calculations are performed assuming a uniform distribution of void. A method of evaluating the presence of holes in a core region has been developed by Behrens.[12] Behrens has developed formulas that describe the increase in migration area as a function of the shape and distribution of the holes, neglecting end effects.

Wachspress has derived an expression for the effective diffusion coefficient, D_c, for a cylindrical hole surrounded by a diffusion medium possessing a cosine axial flux distribution:[13]

$$D_c = \frac{r}{2}\left(\ln \frac{H}{r} - 0.705\right) \qquad (4)$$

where:

r = radius of the hole

H = active axial length of the hole, H being $>10r$

Based on Equation 4, a correction for the finite length of holes has been made to Behren's formula. The factor, γ, that is used to increase the neutron age and thermal-diffusion length squared with a correction for end effects is:

$$\gamma = \left\{ 1 + 2\phi + \frac{\phi^2 \left(\frac{2r}{\phi \lambda_t}\right)}{\exp \frac{2r}{\phi \lambda_t} - 1} + \frac{Q r \phi}{\lambda_t} \right\} \left\{ 1 + \phi \left(\frac{\pi}{2}\right)^2 \frac{r}{H} \left[\ln \frac{H}{r} - .705 \right] \right\} (1-v)^2 \quad (5)$$

where:

v = void fraction

$\phi = \frac{\text{void fraction}}{\text{material fraction}} = \frac{v}{1 - v}$

r = hydraulic radius

λ_t = transport mean free path

H = height of active core

Q = function of the shape of the hole (as defined in Behren's paper[12])

In calculating the three group constants, the increase in age and thermal-diffusion length is applied as a correction factor to the diffusion coefficient, D, in each neutron group.

6. PDQ Code[5]

For all experiments that have been analyzed in this report, fairly coarse mesh spacings have been used in order to minimize the cost of each problem. For most problems, the standard that was adopted was to use one mesh space in each direction for each boiler fuel rod, two to three mesh spacings in each direction for the superheater elements, and two mesh spacings for the water-channel region. The convergence criterion that has been adopted is to use a value of epsilon = 0.05 to terminate the iteration cycle.

The rod-by-rod power distributions for the pure boiler and boiler-superheater arrangements have been normalized to an average power per rod of unity.

All rods are associated with a unit cell. The dimensions of the unit cell for the boiler and superheater are shown in Figure 2. The resulting power distributions are averaged over each cell to find the average power density of the cell. For a core composed of identical

fuel rods, the rod power is directly proportional to the power density. For the superheater and boiler arrangements, the rod-by-rod power for each region normalized to an average rod power of unity is:

Superheater

$$\text{Power/rod} = \frac{P_s A_s \left(1 + \frac{N_b}{N_s}\right)}{A_s \bar{P}_s + A_b \bar{P}_b}$$

Boiler

$$\text{Power/rod} = \frac{P_b A_b \left(1 + \frac{N_s}{N_b}\right)}{A_s \bar{P}_s + A_b \bar{P}_b}$$

where the subscripts s and b refer to the superheater and boiler regions respectively and where:

N = number of rods in the fuel region

P = power density per rod

$\bar{P}$ = average power density per rod

A = total area of fuel region

All of the above quantities are part of the output routine of the PDQ code.

B. Interpretation of Critical Experimental Results

The performance of critical experiments will usually involve techniques that require interpretation before the measurements can be reduced to the desired form. For the initial NUSU experimental program, a partial water-height technique was used to obtain criticality and to measure reactivity changes. In order to convert these measurements to an axial buckling, an expression describing the reflector savings of the upper unmoderated part of the core has to be developed. Also, although the power distributions are measured directly by counting the gamma activity in the fuel rods for the boiler-superheater arrangement, a significant correctional factor has to be applied to account for the larger gamma self-shielding factor of the superheater rod

relative to the boiler rod.

1. Partial Water-Height Analysis

NUSU axial power distribution measurements at various radial positions have shown that the separability of the radial and axial flux distributions that is usually assumed in the solution of the diffusion equations is maintained as the water level is changed.[14] It then becomes feasible to attempt to describe the unmoderated fuel region above the moderator level by an effective reflector savings which can then be used in the determination of the axial buckling. In order to determine the reflector savings, the transient measurements involving the reactivity change with water height were examined for the Yankee[7] and NUSU critical experiments, and an empirical expression was derived.

a. Determination of dk/dh Analytically

Assuming separability of radial and axial fluxes, dk/dh is the following:

$$dk/dh = \frac{2}{(h + \delta_l + \delta_u)} B_Z^2 \left(\frac{\tau_1}{1 + B^2 \tau_1} + \frac{p \tau_2}{(1 + B^2 p \tau_2)} + \frac{L^2}{(1 + B^2 L^2)} \right) \left(1 + \frac{d \delta_u}{dh} \right) \qquad (6)$$

where:

h = height of water above the active fuel

δ_l = reflector savings associated with bottom of the core

δ_u = reflector savings associated with upper section of the core

τ = age

L = thermal-diffusion length

p = average resonance escape probability

B^2 = total geometric buckling

B_Z^2 = axial buckling

The reflector savings for the bottom of the core are assumed to be the same as the radial savings. The reflector savings for the unmoderated fuel rods above the water level, δ_u, is determined empirically by comparing the prediction of Equation 6 with experiment.

b. Determination of the Reflector Savings for the Unmoderated Fuel

It has been assumed that the reflector savings of the unmoderated fuel region, δ_u, has the following form for a region containing UO_2 rods of 10.35 g/cm^3, with stainless-steel and aluminum cladding and with structural material:

$$\delta_u = \frac{2}{3}\bar{\lambda} + C\left[A_{UO_2} + \frac{3}{4}A_{ss} + \frac{1}{3}A_{al}\right] \tanh\left(1 - \frac{h}{H}\right) \qquad (7)$$

where:

$\bar{\lambda}$ = transport mean-free path of the core averaged over all three neutron groups

A = fraction core area occupied by each material

H = active length of fuel

h = water height above active fuel

C = constant to be determined from experiment = 24

The tanh function that is used in Equation 7 has no particular theoretical significance, although it does gives a better fit to data than a linear dependence. The relative worth of stainless steel and aluminum to UO_2 is based on the transport, absorption, and fission cross-sections of these materials.

The value of the constant C determined from the experiments is 24. Substituting this value of C in Equation 7 and using Equation 6, a comparison is made with the Yankee experiment (part d of this section) and the NUSU experiment (Section IV-B). The agreement is of the order of 10 per cent low for one experiment, and 10 per cent high for the other experiment. It is not clear why these differences exist between the two experiments and the theory, as they are larger than any apparent error (in Equation 7) could produce. The main difference in the two experiments was in the method of measuring the change of water height, which could explain the disparity.

However, it should be noted that for the small cores used in the NUSU experiment with relatively large water heights (minimum heights on the order of 2 feet), the criticality measurements are relatively insensitive to the savings produced by the upper fuel region (see Equation 7). For example, at 27 inches, the reflector savings of the upper core is 5 cm and the reactivity worth of an additional 10 centimeters of water is 1 per cent Δk. Thus, a 20 per cent error in determining δ_u would only result in 0.1 per cent Δk error in the determination of the reactivity. This uncertainty decreases with increased water height. Thus, for the purpose of evaluating the analytical criticality predictions, the critical water height technique is quite accurate. If it is desired to fully evaluate the dk/dh analysis, much more refined measurements and analyses should be made to determine the effects of fuel and structural materials in the unmoderated fuel region.

c. Determination of dk/dh Experimentally

The reactivity associated with a change in water height is determined by the e-fold period of the reactor, which is then converted into reactivity by means of the inhour equation. The following formula transforms the measured reactor period into reactivity:

$$\Delta k = \beta^{235} \sum_{i=1}^{6} \frac{1 + \dfrac{(\beta\nu)^{238}}{(\beta\nu)^{235}} \dfrac{A_i^{238}}{A_i^{235}} \delta}{1 + \dfrac{\nu^{238}}{\nu^{235}} \delta} \frac{A_i^{235}}{1 + \lambda_i T} \qquad (8)$$

where:

T = reactor period in seconds

λ_i = the decay constant of i^{th} delayed-neutron group

A_i = the yield of the i^{th} delayed-neutron group normalized such that $\sum_i A_i = 1$. Superscripts represent the yields from U^{235} or U^{238} fissions. The yields are taken from ANL-5800[15], the yield from thermal neutrons being chosen for U^{235}

$\beta\nu$ = the total delayed neutron yield per fission

ν = the number of prompt neutrons per fission as an approximation

$$\nu^{25} = \nu^{28} = 2.46$$

δ = the ratio of U^{238} fission to U^{235} fission in the lattice

$\delta = \frac{\nu^{25}}{\nu^{28}_{-1}} (\epsilon - 1) = 1.685 (\epsilon - 1)$, where ϵ is the fast-fission factor

$\bar{I}$ = a quantity expressing the ratio of "importance" of delayed neutrons to prompt neutrons in the fission cycle.

$\bar{I} = \frac{1 + B^2 \tau_1}{1 + 0.0727 B^2 \tau_1}$, where B^2 is the total geometrical buckling of the core; τ_1 is the age of the fast group in the core; and the 0.0727 factor is found by averaging the first group age of the delayed-neutron groups.

Equation 8 is the same formulation used for the analysis of the Yankee critical experiments[8] with the exception that the importance factor is calculated differently. The above method calculates the importance of delayed neutrons to be about 5 per cent higher than the Yankee values.

d. Comparison with Yankee Experimental Determination of dk/dh With Theory

The Yankee critical experimental measurements[8] were used to evaluate the predictions of Equation 6 using Equation 7 to determine the reflector savings of the unmoderated fuel region.

For three different water heights of both the 2.2 to 1, and 3.9 to 1 water-to-uranium metal experiment, the comparison of the

quoted experimental values with theory was obtained, as listed in Table I.

If the importance of delayed neutrons had been calculated by the method used in this paper, all the quoted Yankee experimental values of dk/dh would be about 5 per cent higher. Thus, it appears that the theory is systematically low by about 10 per cent. However, as will be shown in the analysis of the NUSU experiments, the theoretical values tend to be high. Also, the experimental errors quoted only consider statistical errors. Since the change in water height for these transient measurements is of the order of 1/4 inch to 1/2 inch, an error of 0.01 inch in determining the critical water height corresponds to a 2 per cent and 4 per cent experimental error, respectively.

2. Multizone Power Distributions

In determining the power distributions, only small sections of the core were measured (15 per cent of the fuel rods in one quadrant). The measurements were performed by using the measured gamma activity of one rod as a monitor; the power of all the other rods was determined with respect to the monitor by measuring the relative gamma activities. For the comparison between theory and experiment, the average power of all the measured boiler fuel rods was normalized to the same average power as the corresponding calculated boiler rods. When only boiler fuel is used, these measured activities are proportional to the power. For the case of superheater and boiler fuel, the higher gamma self-shielding of the larger superheater rods requires that an experimental correction factor be applied to the power generation of the superheater rod relative to the boiler rod. This correction factor was determined by examining the five calculated superheater and boiler arrangements which did not contain control rods. The factor which made the measured ratio of the measured rods at the interface between the boiler and superheater region agree with the analyses was found. In this manner, a value of 1.15 ± 0.02 was determined. Two other determinations, one which estimated the gamma self-shielding factors for measured gamma

TABLE I. COMPARISON OF QUOTED YANKEE DIFFERENTIAL WATER-HEIGHT REACTIVITY MEASUREMENTS WITH THEORY

Yankee 2.2/1 Experiment

h (cm)	(Δk/cm) Experiment	(Δk/cm) Theory
89.1	$7.16 \pm 0.19 \times 10^{-4}$	6.62×10^{-4}
70.9	$12.39 \pm 0.31 \times 10^{-4}$	11.43×10^{-4}
62.3	$16.82 \pm 0.46 \times 10^{-4}$	15.44×10^{-4}

Yankee 3.9/1 Experiment

h (cm)	(Δk/cm) Experiment	(Δk/cm) Theory
64.0	$14.39 \pm 0.45 \times 10^{-4}$	14.18×10^{-4}
54.6	$21.60 \times 0.20 \times 10^{-4}$	20.67×10^{-4}
49.5	$26.28 \pm 0.51 \times 10^{-4}$	25.85×10^{-4}

spectra of the rods, and the other which used foil measurements to normalize the power in each rod, indicate a correction factor of similar magnitude. In the results reported here the factor 1.15 has been used to convert the ratio

$$\frac{\gamma \text{ activity reading of superheater rod}}{\gamma \text{ activity reading of boiler rod}}$$ to the ratio

$$\frac{\text{power per unit length of superheater rod}}{\text{power per unit length of boiler rod}}.$$

III. EXPERIMENTAL PROGRAM*

A detailed description of the reactor facility which includes the mechanical design of the core can be found in reference 2.

A. Core Composition and Unit Cell Dimensions

The fuel for both the boiler and superheater regions consists of a high-density 10.35 g/cm^3 sintered uranium dioxide. The U^{235} enrichment of the boiler fuel is 1.85 wt.%, and some experiments were performed which included naturally enriched uranium, 0.714 wt.% U^{235}. The superheater fuel has a U^{235} enrichment of 3.41 wt.%. The boiler fuel is clad with 24.1 mil aluminum. The superheater fuel is clad 18.5 mil stainless steel and the fuel rod is positioned within a 32 mil stainless steel tube. The dimensions of fuel and cladding as derived from actual measurements and the chemical analysis of the compositions are given in Tables II and III. The arrangement of a unit cell together with structural dimensions are shown in Figure 2. In addition to fuel, control rod materials, in the form of slabs, and borated rods are used in some of the measurements. The compositions and dimensions of the control "rods" and borated rods are shown in Table IV.

1. Boiler Region Fuel Assemblies (Figure 3)

The grids in the boiler region were designed to position the boiler rods within a 0.625-inch-square-pitch lattice. The fuel assembly that was used for most of the measurements consisted of a 32-rod 1.85 wt.% U^{235} enrichment which consists of a 6 x 6 lattice with the central four rods missing. The water channel between fuel assemblies is equal to the fuel-rod pitch of 0.625 in. Other experiments were carried out with core configurations that contain variations of the 32-rod assemblies. These measurements included the inserting of aluminum water displacers between the fuel rods and in the water hole in the center of the assembly, substituting natural-uranium rods at the corners of the 1.85 wt.% U^{235}

*The cooperation and assistance of R. S. Harding of Combustion Engineering, Inc. for providing experimental data prior to publication is gratefully acknowledged.

TABLE II. BOILER FUEL RODS

Dimensions

Fuel

Enrichment, wt.%	1.85 ± 0.01
Form	Sintered UO_2 pellets
Diameter, in.	0.445 ± 0.001
Length/pellet, in.	0.650 ± 0.010
Density/pellet, g/cm^3	10.35 ± 0.10
Active fuel length, in.	48

Cladding

Type	6061 Aluminum
Tubing	
Inside diameter, in.	0.4553
Outside diameter, in.	0.5035
Wall thickness, in.	0.0241

Chemical Analysis

Fuel

Uranium content	88.13 wt.%
Oxygen-to-uranium ratio	2.00 - 2.01

Impurities	(ppm)
Si	<50
Ni	33
W	<50
Fe	67
Cu	< 5
Pb	< 2
Cr	<20
Sn	< 2
B	<.3
Cd	< 1
Mo	< 3
Ag	<.2
Ca	<50
Mg	<10

Cladding

Element	(wt.%)
Si	0.60
Mn	0.06
Cu	0.39
Mg	0.86
Ti	0.03
Zn	0.11
Cr	0.28
Fe	0.29
Ni	<0.01
Mo	<0.01
Pb	<0.01
Sn	<0.01
Sb	<0.01
Bi	<0.01

TABLE III. SUPERHEATER FUEL RODS

Dimensions

Fuel		Cladding	Coolant Tubes
Enrichment, wt.%	3.41 ± 0.03	Type	316 SS 316 SS
Form	Sintered UO_2 pellets	Tubing	
Diameter, in.	0.500 ± 0.001	Inside dia., in.	0.5069 0.7718
Length/pellet, in.	0.750 ± 0.001	Outside dia., in.	0.5439 0.8358
Density/pellet, g/cm^3	10.35 ± 0.10	Wall thickness, in.	0.0185 0.0320
Active fuel length, in.	48		

Chemical Analysis

Fuel

Uranium content	88.0 wt.%
Oxygen-to-uranium ratio	2.01

Impurities	(ppm)
F	<50
Si	200
Ni	510
W	<10
Fe	1,030
Cu	8
Pb	1
Cr	40
Sn	5
B	0.2
Cd	0.2
Mo	50
Ag	<0.01
Ca	80
Mg	40

Cladding and Tubing

Element	wt.%
C	0.06
Mn	1.68
P	0.015
Si	0.009
Cr	17.50
Ni	12.50
Mo	2.21
Fe	Remainder

TABLE IV. CONTROL SLABS AND BORON-PYREX RODS

Control Slabs

Material	Width (in.)	Thickness (in.)	g/cm^2
2.15 wt.% boron-stainless steel	7.155 ± 0.010	0.131 ± 0.002	0.0561 (boron)
Cadmium	7.141 ± 0.031	0.020	0.4420
Cadmium	7.156 ± 0.031	0.040	0.9130

Boron-Pyrex Annular Rods

Inside diameter (glass)	0.237 in.
Outside diameter (glass)	0.321 in.
Inside diameter (aluminum clad)	0.370 in.
Outside diameter (aluminum clad)	0.500 in.
Density of glass	2.216 g/cm^3
Boron content	3.625 wt.% boron
Water content	Remaining area inside clad

assembly. Measurements were also performed on a 36-rod element core in which the effect resulting from the removal of two corner rods and their replacement with borated rods, was investigated.

Some explanation is in order as to the reason for the choice of the 32-rod assembly. This fuel assembly is based on BONUS core design[3,4] which indicated the peak-to-average power of this element is about 10 per cent less than for the 36-rod element which uses about 10 per cent more fuel. Thus, initially, the same total power will be generated by both elements. This conclusion has been sustained by the experimental power measurements. For actual power reactor operation, the 32-rod assembly with its higher neutron parasitic absorption will require a higher U^{235} burnup allowance than the 36-rod assembly. However, if the burnup of the assembly is limited by the burnup of the hottest rod within the assembly and if the relative initial cell power distributions of the two types of elements tend to sustain themselves, then the 32-rod element can generate the same total heat output as the 36-rod element. Since the cost of fuel fabrication is the major fraction of the total cost, there appears to be a net economic gain to design a fuel element with inherent power flattening.

2. Superheater Region Fuel Arrangement (Figure 4)

All the rods are positioned on a 1.094-inch-square pitch. Each rod is surrounded by a steam coolant tube. These rods are arranged in an 8 x 32 array and are divided into four sections, each section contains a 2 x 32 array of rods. Each section is capable of being flooded and voided independently of the other sections; the spacing of rods between sections is the same as the spacing of rods within the section. Figure 4 shows the geometric arrangement of the entire superheater region.

The superheater simulates one quadrant of the BONUS superheater arrangement. The particular design, involving single rods in coolant tubes, was formulated for the BONUS reactor to prevent fuel melting upon a loss of coolant followed by a reactor scram, by allowing each rod to radiate heat to the surroundings. This element is over-moderated, since the mechanical design required to satisfy the shutdown coolant requirement necessitates a water-to-fuel ratio that is considerably larger than is desired solely on the basis of nuclear considerations.

B. Experimental Arrangements and Measurements[14]

The nuclear properties of three general areas were evaluated — the boiler, the boiler with fully inserted control rods, and the boiler and superheater with and without fully inserted control rods. In all measurements, criticality is attained by adjusting the water height of the core. Power distributions were determined by directly measuring the activation of the fuel rods.

1. Boiler Region

The individual fuel assemblies and their geometrical arrangements within the core are shown in Figures 3 and 5. The basic fuel rod within the assembly possesses 1.85 wt.% enriched U^{235}. The following fuel assemblies have been used in the course of the experiments:

a) a 32-rod assembly;
b) a 32-rod assembly with 16-1/4-inch aluminum water displacers between fuel rods in each assembly;
c) a 32-rod assembly with 4-1/2-inch aluminum water displacers at the center of each assembly;
d) a 32-rod assembly with natural-uranium rods at the corner positions;
e) a 32-rod assembly containing all natural-uranium rods;
f) a 34-rod assembly;
g) a 34-rod assembly with two borated rods occupying the corner positions;
h) a 36-rod assembly.

2. Boiler Region With Control Rods

Two thicknesses of cadmium and borated-stainless steel slab type control rods were evaluated for the case of full rod insertion into the core; Figure 6 shows the geometrical arrangement for these measurements which are, as follows:

a) A 20-mil cadmium slab, 7-1/8 inches wide, taped to a 1/8-inch aluminum slab;

b) a 40-mil cadmium slab, 7-5/32 inches wide, taped to a 1/8-inch aluminum slab;

c) a 0.131-inch 2.15 wt.% boron-stainless steel slab, 7-1/8 inches wide;

d) a 0.262-inch 2.15 wt.% boron-stainless steel slab, 7-1/8 inches wide.

3. Boiler and Superheater Regions

a. Internal Superheater

Figure 7 shows the arrangement of the internal superheater with respect to the boiler for the case of no-control-rods and with two 0.131-inch 2.15 wt.% boron-stainless steel rods fully inserted. The reactivity effects of partial and complete withdrawal of water from the superheater region were measured.

b. External Superheater

Figure 8 shows the arrangement of the external superheater with respect to the boiler for the case of no-control-rods and with two 0.131-inch 2.15 wt.% boron-stainless steel rods fully inserted. The reactivity effects of partial and complete withdrawal of water from the superheater region were measured.

IV. COMPARISON OF THEORY AND EXPERIMENT

For the core compositions and lattice arrangements given in Tables II through IV and Figures 2 through 8, the reactivity and power distributions were calculated and compared with experiment. For most of the experiments, the predicted critical water height and power distributions were calculated in advance of the measurement.

The experimental power distribution for each rod was measured at three axial points -- at approximately half-water height and at 4 inches above and below the half-water height. These three values were averaged for each rod to determine the radial power distribution.

A. Reactivity and Power Distributions

1. Boiler Region

The boiler region consists of fuel rods of 1.85 wt.% U^{235} enrichment unless otherwise noted. The arrangement of the fuel within an assembly is shown in Figure 3, and the arrangement of fuel assemblies is shown in Figure 5.

a. A Twenty-four-Assembly Core

Six different fuel assemblies were analyzed. These assemblies contained 32 rods, 34 rods, 36 rods, 32 rods with 16-1/4-in. aluminum rods, 32 rods with 4-1/2-in. aluminum rods, and 34 rods with two boron-pyrex corner rods. For the boron-pyrex assembly measurement, the central four assemblies possessed the boron-pyrex rods, and the remaining assemblies contained 36 rods. In all other measurements, the core consisted of 24 identical assemblies. The calculated reactivities and the comparison with experiment are shown in Table V.

The calculated rod-by-rod radial power distributions for the above cases are given in Figures 9 through 14. The experimental power distribution measurements were only performed for the 32-rod, 36-rod, and boron-pyrex rod cases. In the figures, each square

TABLE V. THE CALCULATED AND MEASURED REACTIVITIES OF A CORE CONSISTING OF TWENTY-FOUR BOILER FUEL ASSEMBLIES WITH DIFFERENT FUEL AND MATERIAL ARRANGEMENTS WITHIN THE ASSEMBLY

Fuel Assemblies	h (cm)	Reactivity (Calculated)	Reactivity (Measured)
32-rod	68.58	0.9890	1.0000
34-rod	87.73	0.9883	1.0000
36-rod	66.80	0.9883	1.0000
32-rod with 16-1/4-in. aluminum rods	85.75	0.9879	1.0000
32-rod with 4-1/2-in. aluminum rods	80.34	0.9865	1.0000
34-rod, two boron-pyrex corner rods	113.31	0.9855	1.0000

represents one fuel rod, and the number in each square is the relative power per unit length of fuel element at the point of measurement, normalized to an average value of unity.

b. A Twenty-Assembly Core

Measurements were performed on a 32-rod-assembly core in order to observe if any significant changes occur in the reactivity and power distribution as a function of the critical water height.

h (cm)	Reactivity (Calculated)	Reactivity (Measured)
89.33	0.9886	1.0000

The calculated power distribution with the measured comparison is shown in Figure 15.

c. A Twenty-eight-Assembly Core

Measurements were performed on a twenty-eight-assembly core in which each assembly contained 32 rods, the corner rods being naturally enriched.

h (cm)	Reactivity (Calculated)	Reactivity (Measured)
99.11	0.9892	1.0000

The calculated power distribution together with the measured comparison is shown in Figure 16.

d. A Thirty-two-Assembly Core

Measurements were performed on a thirty-two-assembly core in which each assembly contained 32 rods, the central four assemblies being naturally enriched.

h (cm)	Reactivity (Calculated)	Reactivity (Measured)
108.23	0.9886	1.0000

The calculated power distributions together with the measured comparison is shown in Figure 17.

2. Boiler Region With Control Rods

Using the experimental results for the 28-assembly core arrangement in which each assembly contains 32 rods, the value of the epithermal-transmission probability was determined for two different thicknesses of cadmium and borated-steel slabs. The dimensions and composition of the slabs are described in Table IV. The experimental arrangement is shown in Figure 6. In the analysis, the epithermal-transmission probability, T_2, was determined by achieving a reactivity of 0.9883 for the materials listed in Table VI. These values are used in the analysis of the boiler-superheater arrangements.

3. Boiler and Superheater Regions

a. Internal Superheater

A superheater fuel rod has a 3.41 wt.% U^{235} enrichment, and the boiler fuel rod has a 1.85 wt.% enrichment. The experimental internal superheater arrangements are shown in Figure 7. For the configuration in which there is the equivalent of 14 boiler assemblies on each side of the boiler, the partial water height was calculated for the superheater completely voided and flooded. In addition, the case of the middle two superheater sections voided and the outer two flooded and the case of the middle two superheater sections flooded and the outer two sections voided were also measured and calculated, as listed in Table VII.

The calculated rod-by-rod power distributions together with the measured power distributions for the superheater and the entirely voided and entirely flooded conditions are shown in Figures 18 and 19, respectively. As before, the number in each square is the relative power per unit length of fuel rod, at the point of measurement. The total calculated power generation in the superheater is listed in Table VII.

An internal superheater arrangement with two control rods was also measured. For this measurement, there were 16 boiler assemblies on one side of the superheater and the equivalent of 19 boiler assemblies on the other side. Two 0.131-in. 2.15 wt.% boron-stainless steel 7-1/8-in. slabs were completely inserted, one on each side of the superheater,

TABLE VI. THE EPITHERMAL TRANSMISSION PROBABILITIES OF CADMIUM AND BORON-STAINLESS STEEL AS DETERMINED FROM CRITICALITY EXPERIMENTS

Control-rod material	h(cm)	g/cm^2	T_2
Cadmium (20 mil)	93.57	0.442	0.956
Cadmium (40 mil)	95.25	0.913	0.930
2.15 wt.% borated-stainless steel (0.131 in.)	99.16	0.0561	0.883
2.15 wt.% borated-stainless steel (0.262 in.)	109.04	0.1123	0.825

TABLE VII. THE CALCULATED AND MEASURED REACTIVITY AND THE CALCULATED SUPERHEATER POWER OF THE INTERNAL BOILER-SUPERHEATER ARRANGEMENT AS A FUNCTION OF THE AMOUNT OF WATER IN THE SUPERHEATER

	h	Reactivity (Calculated)	Reactivity (Measured)	Superheater Power (% of Total Reactor Power) (Calculated)
Entirely Voided	71.20	1.0051	1.0000	38.3
Inner two sections flooded Outer two sections voided	73.38	1.0047	1.0000	40.3
Inner two sections voided Outer two sections flooded	77.60	1.0049	1.0000	39.7
Entirely flooded	81.94	1.0038	1.0000	41.2

between the boiler and superheater regions. Only the completely voided condition was analyzed.

h (cm)	Reactivity (Calculated)	Reactivity (Measured)	Superheater Power (% of Total Reactor Power) (Calculated)
80.24	0.9990	1.0000	31.6

A comparison of the calculated and measured rod-by-rod power distribution for this configuration is shown in Figure 20.

b. External Superheater

The same fuel assemblies that were employed for the internal superheater measurements were used for the external superheater measurements. The experimental arrangements are shown in Figure 8. There were 24 boiler assemblies adjacent to the superheater region. Calculations were performed for the superheater either completely voided or completely flooded. An additional measurement in which the separation between the boiler and superheater was increased one inch to 1.81 in. was also analyzed for the voided condition, as listed in Table VIII.

A comparison of the calculation and measured rod-by-rod power distribution for these cases is shown in Figures 21, 22, and 23. The total calculated power generation in the superheater is listed in Table VIII.

An external superheater arrangement with control rods was also measured. For this experiment, the same amount and arrangement of fuel was used as for the no-rod measurements. Two 7-1/8-in.-wide and 0.131-in.-thick 2.15 wt.% boron-stainless steel rods were inserted between the boiler and superheater. Only the completely voided superheater region was analyzed.

h (cm)	Reactivity (Calculated)	Reactivity (Measured)	Superheater Power (% of Total Reactor Power) (Calculated)
80.04	0.9915	1.0000	22.4

A comparison of the calculated and measured rod-by-rod power distributions for this configuration is shown in Figure 24.

TABLE VIII. THE CALCULATED AND MEASURED REACTIVITY AND THE CALCULATED SUPERHEATER POWER OF THE EXTERNAL BOILER-SUPERHEATER ARRANGEMENT

	h (cm)	Reactivity (Calculated)	Reactivity (Measured)	Superheater Power (% of Total Reactor Power) (Calculated)
Voided superheater	59.74	0.9918	1.0000	26.6
Flooded superheater	59.52	0.9937	1.0000	28.4
Voided superheater (1.81 in. boiler-superheater channel)	72.80	0.9935	1.0000	22.8

B. Partial-Level Height Reactivity Measurements

The calculation of dk/dh has been made using Equation 6. The experimental values of dk/dh have been determined by measuring the period induced by a change of water height. The conversion to reactivity is accomplished by using Equation 8.

For the boiler region, the comparison between the theoretical and experimental values of dk/dh were obtained, and are listed in Table IX.

TABLE IX. COMPARISON BETWEEN THE THEORETICAL AND EXPERIMENTAL VALUES OF dk/dh FOR THE BOILER REGION

Twenty-four-Assembly Core

	h (cm)	dk/dh (Δk/cm) (Calculated)	dk/dh (Δk/cm) (Measured)
32-rod	68.58	12.70×10^{-4}	11.48×10^{-4}
34-rod	87.73	6.90×10^{-4}	6.51×10^{-4}
36-rod	66.80	13.34×10^{-4}	12.48×10^{-4}
32-rod, 16-1/4-in. aluminum rods	85.75	7.64×10^{-4}	7.13×10^{-4}
32-rod, 4-1/2-in. aluminum rods	80.34	9.00×10^{-4}	7.69×10^{-4}
34-rod, two boron-pyrex corner rods	113.31	3.59×10^{-4}	3.23×10^{-4}

Twenty-Assembly Core

h (cm)	dk/dh (Δk/cm) (Calculated)	dk/dh (Δk/cm) (Measured)
89.33	6.53×10^{-4}	6.21×10^{-4}

Twenty-eight-Assembly Core With Natural-Uranium Corner Rods

h (cm)	dk/dh (Δk/cm) (Calculated)	dk/dh (Δk/cm) (Measured)
99.11	5.10×10^{-4}	5.04×10^{-4}

Thirty-two-Assembly Core With Four Central Natural-Uranium Assemblies

h (cm)	dk/dh (Δk/cm) (Calculated)	dk/dh (Δk/cm) (Measured)
108.23	4.08×10^{-4}	3.55×10^{-4}

Twenty-eight-Assembly Core With Control Rods

Control-rod material	h (cm)	dk/dh (Δk/cm) (Calculated)	dk/dh (Δk/cm) (Measured)
Cadmium (20 mil)	93.57	5.83×10^{-4}	4.94×10^{-4}
Cadmium (40 mil)	95.25	5.56×10^{-4}	5.24×10^{-4}
2.15 wt.% borated-stainless steel (0.131 in.)	99.16	5.03×10^{-4}	4.93×10^{-4}
2.15 wt.% borated-stainless steel (0.262 in.)	109.04	3.94×10^{-4}	3.65×10^{-4}

V. DISCUSSION OF RESULTS

A. Significance of the Comparison Between Theory and Experiment

1. Boiler Arrangements

The agreement between theory and experiment is good. The reactivity calculations are within -1.5 per cent Δk of criticality, or there is more reactivity present than calculated in all cases. The agreement in rod-by-rod power distributions is equally good; a comparison between theory and experiment indicates differences of the order of 5 per cent or less which corresponds to the experimental accuracy.

Furthermore, it should be noted that the changes that occur in reactivity and power distributions by comparing small changes within the fuel assemblies are very well reproduced. The 32-rod assembly with equal amounts of aluminum between fuel rods and at the center of the assembly would be calculated to have the same reactivity if a homogenized fuel assembly calculation were performed. However, these calculations show the aluminum in the center of the assembly to be 0.5 per cent more reactive, thus agreeing with the measurement. Even more evident is the fact that by removing two corner rods of the 36-rod assembly the reactivity is reduced by approximately 1.5 per cent Δk. If the other two corner rods were removed to make a 32-rod element, this type of element would be approximately 2.8 per cent Δk less reactive than the 32-rod element with corner rods, but with the four fuel rods removed from the center of the assembly. However, calculations which would homogenize the water, inside and outside of the element, with the fuel would calculate these elements to have precisely the same reactivity.

Varying the arrangement of fuel within an assembly indicates the sensitivity of calculations to evaluating local power distributions. The rod-by-rod power distributions which implicitly includes water-channel effects accurately describes the situation. The measurements with natural-uranium corner rods and with poison corner rods used a unit

cell analysis for these regions with very satisfying results. The comparison of the characteristics of the 32-rod and 36-rod assemblies shows that the predicted 10 per cent lower peak-to-average in the 32-rod element is corroborated by the measurements. Thus, the power-flattening introduced by the moderator at the center of the assembly allows the 32-rod element with approximately 10 per cent less fuel to produce the same total power as the 36-rod element.

2. Control-Rod Arrangements

The epithermal-transmission factors determined for boron and cadmium indicate a considerably smaller epithermal effect for these lattices than is present with a fully enriched core.[11] Further measurements with more complex configurations are desired before the accuracy of the control-rod calculations can be separated from the other uncertainities in the calculations. Such measurements which will also include partial rod insertion are being planned for the BONUS Critical Mockup Experiments which will use essentially the same fuel as the initial NUSU Critical Experiments.

3. Superheater and Boiler Arrangements

These measurements require a substantial fraction of boiler fuel in order to achieve criticality. Therefore, the analysis of the nuclear characteristics of the superheater region necessarily include the effects of the boiler region. On the surface, the experiments involving both the boiler and superheater fuel appear closer to the theoretical reactivity predictions than the experiments that were concerned only with boiler fuel. All measurements, including those that involve control rods, agreed to within -1.0 per cent Δk to +0.5 per cent Δk. However, the reactivity of the superheater has been somewhat overestimated relative to the boiler.

For the internal superheater arrangement where no control rods are present, the superheater region has the highest statistical weight of any of the measurements as is shown by the power split between boiler and superheater. The absolute reactivity predictions for these cases

possessed about 1.5 per cent Δk less reactivity compared with that of the measurements solely containing boiler fuel. Nevertheless, the power distributions are very well reproduced for the no-control-rod cases. With control rods present, the internal superheater core arrangement is assymetric with more boiler fuel on one side than on the other. The reactivity is predicted quite well, but there is flux tilt to the side with more boiler fuel and the power distributions are not in nearly as good agreement.

For the external superheater arrangement, the superheater has a much lower statistical weight, and the reactivity characteristics tend to be that of the boiler region. The absolute reactivity prediction differs by only a few tenths of a percent Δk from the pure boiler fuel measurements. However, the measured power generation in traversing the superheater is falling off faster in a radial direction than the calculations predict. These radial power distributions show that the material buckling of the superheater has been somewhat overestimated by the calculations. Therefore, the deviation in the reactivity prediction compared with that of the pure boiler measurements is directly attributable to the superheater constants and not the large water channel existing between the boiler and superheater regions. Since the superheater fuel assembly has a much higher water-to-fuel ratio than any element that has been calculated heretofore, the higher reactivity calculated for the superheater could be attributed to errors in the analysis. However, the reactivity changes associated with voiding and flooding of the superheater are in good agreement, and tend to substantiate the analytical methods. The deviations between theory and experiment could also be explained by uncertainties in the superheater core compositions. The dimensions of the superheater element, including the U^{235} enrichment and the total amount of steel, are subject to greater uncertainties than the corresponding quantities in the boiler element. This possibility is discussed in the next section. For the BONUS Mockup Critical Experiments, three additional superheater sections will be used. There will be a closer inspection of the materials and dimensions. Similar experimental measurements will be made, and the accuracy of the calculations can then be better evaluated.

It will be noted that for the external superheater arrangement, there is essentially no change in reactivity upon complete voiding and flooding of the superheater. The explanation for this phenomenon is that this element is overmoderated, and the gain in reactivity which occurs upon the voiding of elements is just compensated by the increased leakage from the core. With the internal superheater, the negative leakage effect is reduced and there is a net gain of reactivity upon voiding of about 1 per cent Δk. Thus, in order to satisfy the safety requirements for this type of element, it is best to have the superheater on the outside of the core. Obviously, one cannot generalize this result to other superheater elements. In fact, from the nuclear standpoint, one could adjust the fuel arrangement including enrichment, water-to-fuel ratio, and nuclear poisons to obtain the desired reactivity change at a prescribed core condition for any other arrangement of the superheater region.

4. Boiler-Superheater Control Systems

For the BONUS reactor project, a conventional type of control system is being used. Control rods positioned in the boiler and between boiler and superheater are being used to control reactivity and the division of power between the boiler and superheater. The experiments on the internal and external superheater with control rods between boiler and superheater regions show the effect of the rods on reactivity, power distribution, and power split.

An alternate control system that is particularly applicable to an integral external nuclear superheater is a moving-fuel system in which the superheater region is moved radially with respect to a fixed boiler region.[4] Since the two regions are independent in regard to heat-transfer considerations, the movement of the superheater does not change the flow rate of steam coolant. This type of moving-fuel control system can be used as a safety or safety-shim system but still would require additional control to regulate both the boiler power output and the shutdown safety margin of the reactor.

5. Partial-Level Height Analysis

The calculated values of dk/dh are systematically high by less than 10 per cent compared to the measured values. The reason for this difference is not known, although the calculation may be within the experimental error. The analysis of the Yankee experiment yielded values that were systematically low by the same amount. The fact that for a particular geometric arrangement of the NUSU experiments the absolute value of the predicted reactivity remain constant is indicative that the value of the integral, $\int dk/dh\ dh$, is being properly evaluated analytically. However, the prime purpose of the dk/dh analysis is to determine if the reflector savings of the unmoderated fuel region are being calculated with reasonable accuracy. It would seem that the recipe that is used is adequate for the present purposes, i.e., determination of criticality, and measurements of a more detailed nature should be made to fully evaluate the application to small or local reactivity changes.

B. General Observations

1. Application of Analytical Methods to Nuclear Superheat Analysis

The usual nuclear considerations of light-water boiling-water reactors involve total reactivity, power distributions, and stability. Integral nuclear superheat intoduces another variable that has to be satisfied — namely, the power split between the boiler and superheater. As was shown in the analysis of the external superheater, even though the reactivity of the entire core was very close to prediction, the calculation of a split in total power output of the core was less accurately described. Thus, in the design of the integral nuclear superheater, the lifetime of the core may not only be limited by reactivity considerations but also by the ability of each of the regions to produce rated power output.

The specialized nature of the fuel elements used in the NUSU experiments precludes any generalization of these results to an arbitrary core design. However, the analytic methods that have been developed appear to be appropriate to any light-water reactor design

using solid-rod fuel elements. For more complex fuel-element designs, such as those involving annular rods, some different subroutines will be needed to account for the resonance escape and thermal utilization for these elements. However, it is believed that such methods can be incorporated into the general calculational scheme without disturbing the accuracy. Such calculations have been carried out in the design of a large integral boiler-superheater reactor.[16] Critical experiments using highly-enriched fuel show that the calculational accuracy is maintained at elevated temperature.[6] To some extent, the predicted accuracy for an irradiated core can be considered to be outside the range of the cold experiments, although here, too, it is expected that for the appropriate thermal cross sections of the plutonium isotopes and fission products, similar results will be obtained. For the BONUS project post-construction research and development program, it is proposed that a detailed analysis be made on the operating BONUS core to evaluate these analytical methods under operating conditions.

2. Accuracy of Analytical Methods and Determination of Core Composition

If the calculations tend to underestimate reactivity or if there is more reactivity present than calculated, then a minimum of harm is done even though it is disturbing to have any deviation exist between theory and experiment in the determination of reactivity. If the shutdown control is not sufficient, the initial excess reactivity can be reduced by the mechanical insertion of neutron poisons that can be withdrawn at some future time. On the other hand, it may not be possible to increase fuel enrichment or fuel content if there is not sufficient reactivity present.

Uncertainties in the determination of the core composition and geometry serve to limit the accuracy of any core analysis. An additional experiment which would define this uncertainty would be to build a completely new core to the same mechanical, fuel, and material specifications and to repeat the measurements. Obviously, it is too expensive to perform such an experiment. However, observing the uncertainties of dimensions and compositions, the probability of

achieving the same results is small. It is expected that deviations of at least 0.5 per cent Δk would exist between two supposedly exact experimental arrangements and compositions. Thus, a reactor core design should have this mechanical and compositional uncertainty in mind.

The performance of detailed analysis prior to the start of the critical experiments excludes any possible influence experimental results may have on the analysis. In this respect, there is a general misconception as to how the analytical methods can be altered to achieve agreement with measurement. The entire averaging procedures that are used to determine the diffusion parameters are built into a machine code. The same methods are applied to every problem. However, the uncertainties that exist in core composition and geometry can significantly change the input data used to determine the diffusion parameters as well as to change the size of regions within the core. Thus, if there is a known disagreement with experiment, the analyst could rationalize with a reasonably clear conscience that the median compositions and dimensions are, in fact, closer to the tolerances imposed on the composition and dimensions, and achieve better agreement with experiment. In order to remove this source of uncertainty, it is essential that a reasonably high degree of exactness be applied to the materials and their arrangement within the core. Also, one cannot expect a high degree of analytical precision and understanding of the experiments for core configurations that contain a large number of undetermined heterogeneities.

Prior to the start of a core analysis, the core dimensions and compositions should be well defined. However, the actual dimensions and compositions of materials that are inserted into the core may differ significantly from the median specifications used to order the material.

To illustrate, the superheater coolant tubes used in the NUSU experiments had the following specifications and manufacturer's description:

—Outside diameter, 0.833 in.;

—inside diameter, 0.765/0.775 in.;

—wall, 0.029 in.

The measured tube dimensions were the following:

—Outside diameter, 0.8358 in.;

—inside diameter, 0.7718 in.;

—wall, 0.032 in.

Thus, the specified 0.029-in. wall turned out to be 0.032 in., which is the dimension used in the analysis. It remains without saying that this is a very significant increase over the nominal stainless-steel specification.

The NUSU measurements have indicated that the reactivity of the superheater relative to the boiler is less than predicted by the analysis. If there had been 6 per cent more neutron absorption in the steel in the superheater region than the absorption that was computed in the analysis, the agreement between theory and experiment would be exact. A check of the physical constants used for the analysis of the superheater region revealed that a density too low for Type 316 stainless steel was used in the calculation; a value of 8.03 g/cm^3 rather than 7.85 g/cm^3 should have been used. This correction accounts for 2 per cent additional absorption in the steel. An additional 4 per cent absorption could be associated with the uncertainty of the chemical composition of the steel or the total steel content.

C. Effect of NUSU Measurements on BONUS Core Design

The comparisons of experimental and calculational results reported here have shown that the calculational methods described in Reference 1 will calculate the reactivities and power distributions of assemblies similar to the BONUS core to within the limits of uncertainty of the experimental measurements. These uncertainties result primarily from the spread of tolerances on composition and configuration of the experimental assemblies. The effect of such uncertainties must be investigated more thoroughly in the BONUS critical experiments, but the experiments performed under the NUSU program do not indicate a need for

any modification of the analytical procedures that have been used in the BONUS core design to date (e.g. in the calculation of the reactor physics characteristics given in Reference 3), and that will be used for the continuation of the design analysis.

If the experimental uncertainties are ignored and all discrepancies between calculation and experiment are considered, at this point, to reflect uncertainties in the reactor physics design of the reactor, then the current status of accuracy of that design can be assessed approximately as follows:

The calculational methods predict reactivity of assemblies having characteristics similar to the BONUS boiler region consistently, but give predictions that are low by 1% to 1.5% k_{eff}. This discrepancy is considered relatively unimportant because it is a consistent one and therefore should represent only a second order discrepancy in predictions of the important reactivity changes due to such sources as the steam coefficient of reactivity. This assessment is strongly supported by the success of the calculational techniques in predicting the reactivity changes caused by small experimental variations in the lattice arrangement of the critical assemblies. The calculational methods predict power distributions, both intra-cell and inter-cell, in these boiler-type lattices with an accuracy that is quite adequate for design purposes.

In the boiler-superheater combination, the calculations predict gross reactivities that are somewhat closer to those measured, but the over-all indications of the experimental-theoretical comparison are that this may be due to a reactivity prediction for the superheater section that is disproportionately high relative to the reactivity prediction for the boiler section. Again, the existence of a small gross reactivity discrepancy is considered rather unimportant per se; and again the confidence in the utility of the calculation method is strengthened by its success in predicting the reactivity effect of superheater flooding. With regard to the prediction of power distribution, the apparent discrepancy in the reactivity ratio between boiler and superheater manifests itself as a discrepancy in power distribution which becomes

more and more apparent as the outer edge of the superheater is approached. The experimental configuration which shows this effect in closest relation to the actual BONUS operating conditions is that for which the results are given in Figure 21. If a reasonable interpolation is used to extend the experimental measurements indicated on Figure 21 to give a complete experimental map of the superheater power distribution, comparison of this map with the calculated map shows that the calculation predicts a total superheater power which is about seven per cent too high relative to the power density near the center of the boiler region. The same approach shows that the calculation predicts a maximum/average power density in the superheater region which is about five per cent too low. If these discrepancies had to be accepted as real uncertaintites in the BONUS design, they would certainly be undesirable, but probably tolerable. Since a further extensive experimental program is to be conducted, these uncertainties will be greatly reduced. As mentioned above, it is probable that they can be accounted for by discrepancies between the compositions and geometries of the calculated and measured assemblies. If this should prove not to be the case, it would still be possible to remove a large fraction of the uncertainty by a simple correction factor.

The major limitations of the program to date are that the measurements have been made in cold assemblies whereas the important reactor conditions are the hot ones, and that the measurements and analyses have been, on the whole, two-dimensional ones, whereas reactor performance is very strongly dependent on the three-dimensional behavior of the core when it is occupied by partially inserted control rods and a nonuniform distribution of steam voids. There does not appear to be any reason to expect the calculations to be less accurate at high temperatures, except for the "old" reactor in which plutonium isotopes become important.

The problem of three dimensions is one of complexity rather than one of theoretical representation. To the extent that a two-dimensional calculation, such as the PDQ calculation, can be used to give two-dimensional agreement with experiment, there is no reason to

believe that a three-dimensional calculation utilizing the same basic approach would not give equally good three-dimensional agreement. Since a practical three-dimensional code using sufficiently small lattice spacings is not available, the necessary three-dimensional mapping of power for the BONUS reactor, and the prediction of the nuclear behavior of the three-dimensional reactor, will depend heavily upon the BONUS critical experiments.

REFERENCES

1. R. W. Deutsch, Method for Analyzing Low-Enrichment, Light-Water Cores, USAEC Report GNEC 133, General Nuclear Engineering Corporation, October 5, 1960. (To be published in J. Nuclear Energy)

2. R. S. Harding and M. S. Slater, Advanced Critical Experiment Safeguards Report, USAEC Report CEND-105, Combustion Engineering, Inc., Supplement No. 2, 1960.

3. Boiling Nuclear Superheater (BONUS) Power Station, Preliminary Design Study and Hazards Summary Report, Vol. 4, USAEC Report PRWRA-GNEC 2A, (TID-8524), Puerto Rico Water Resources Authority and General Nuclear Engineering Corporation, June 1960.

4. Boiling Nuclear Superheater (BONUS) Power Station, Preliminary Design Study, USAEC Report PRWRA-GNEC 3A, Puerto Rico Water Resources Authority and General Nuclear Engineering Corporation January 8, 1960.

5. V G. Bilodeau, W. R. Cadwell, J. P. Dorsey, J. G. Fairey, R. S. Varga, PDQ - An IBM-704 Code to Solve the Two-Dimensional, Few-Group Neutron Diffusion Equations, USAEC Report WAPD-TM-70, Westinghouse Electric - Bettis Plant, 1957.

6. G. D. Hickman, J. A. Bistline, and L. A. MacNaughton, Water-Moderated Cores with Boron Septa at Elevated Temperatures, Nuclear Sci. and Eng., 8(5): 381 (1960).

7. D. Klein, A. Z. Kranz, G. G. Smith, W. Baer, and J. DeJuren, Measurements of Lattice Parameters in Water-Moderated, Slightly Enriched Lattices, Nuclear Sci. and Eng., 3(4): 403 (1957).

8. P. W. Davison, S. S. Berg, W. H. Bergmann, O. F. Hanlen, B. Jennings, and P. D. Leamer, Yankee Critical Experiments, USAEC Report YAEC-94, Yankee Atomic Electric Company, 1959.

9. R. M. Ball, A. L. MacKinney, J. H. Mortenson, D. A. Ross, and D. V. Williams, Critical Experiments for N.S. Savannah Core, Trans. American Nuclear Society, 1(2); 10 (1958).

10. P. B. Daitch, B. J. McGovern, and M. Schilder, CEPTR, An IBM-704 Code to Solve the P-3 Approximation to the One Velocity Equation in Cylindrical Geometry, USAEC Report MPC-20, 1959.

11. R. W. Deutsch, Evaluation of a Bank of Slab-Type Control Rods, Nuclear Sci. and Eng., 4(3): 322 (1958).

12. D. J. Behrens, The Effects of Holes in a Reactivity Material on the Passage of Neutrons, Physics Society of London Proceedings, 62A: 607 (1951).

13. E. L. Wachspress, Notes on a Streaming Problem, USAEC Report KAPL-ELW-4, Knolls Atomic Power Laboratory, General Electric, 1954.

14. R. S. Harding, NUSU Critical Experiments, Part I, USAEC Report CEND-115, Combustion Engineering, Inc., Dec. 29 (1960).

15. Reactor Physics Constants, USAEC Report ANL-5800, Argonne National Laboratory, undated.

16. A 200-Mw(e) Boiler-Superheater Reactor Preliminary Design, USAEC Report GNEC 136, General Nuclear Engineering Corporation, Dunedin, Florida, October 25, 1960.

ANALYSIS OF THE INITIAL NUCLEAR SUPERHEAT CRITICAL EXPERIMENTS

SUPPLEMENTARY STUDY
RELATED TO BONUS AND NUCLEAR SUPERHEAT PROGRAMS

ILLUSTRATIONS

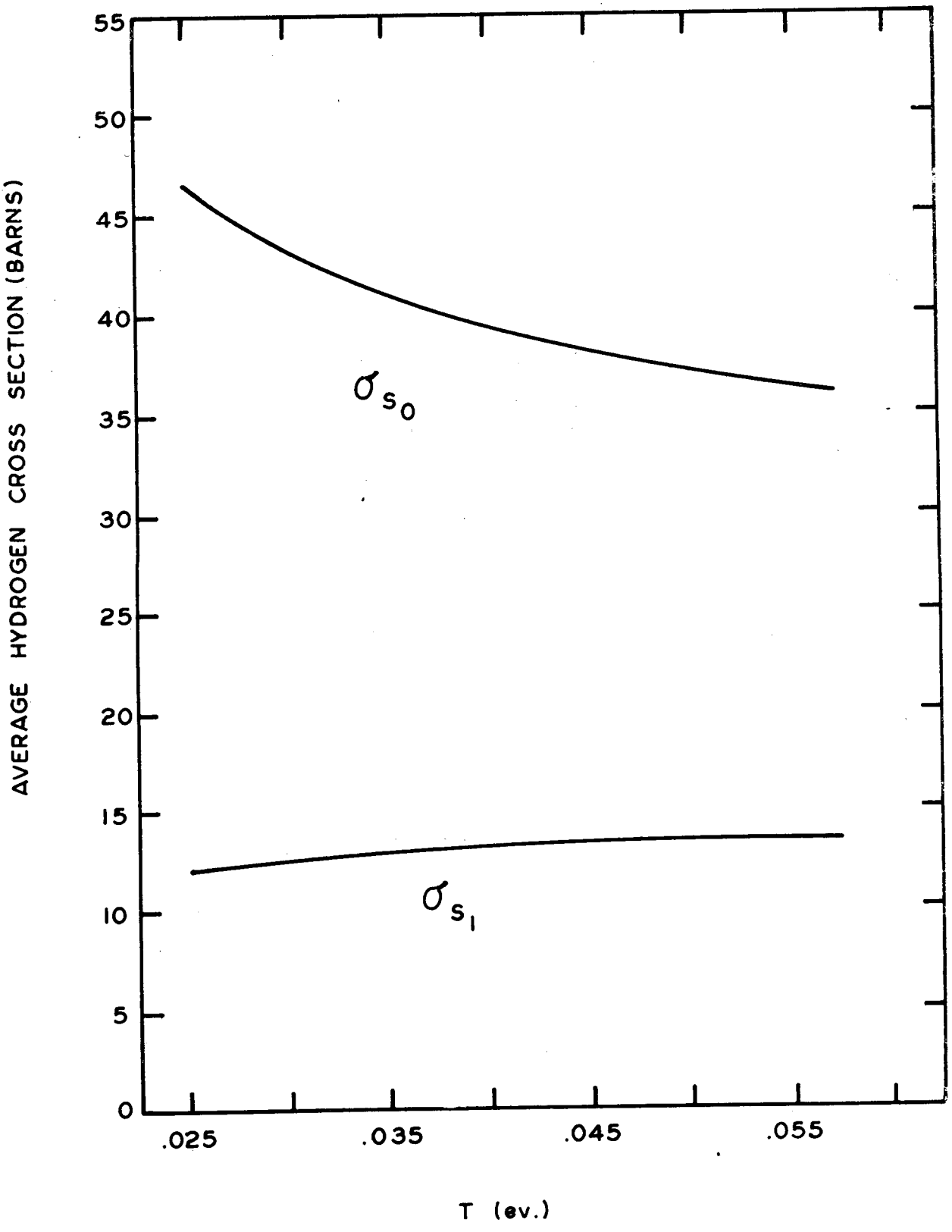

Figure 1. Hydrogen Cross Sections for CEPTR P-3 Calculations[10]

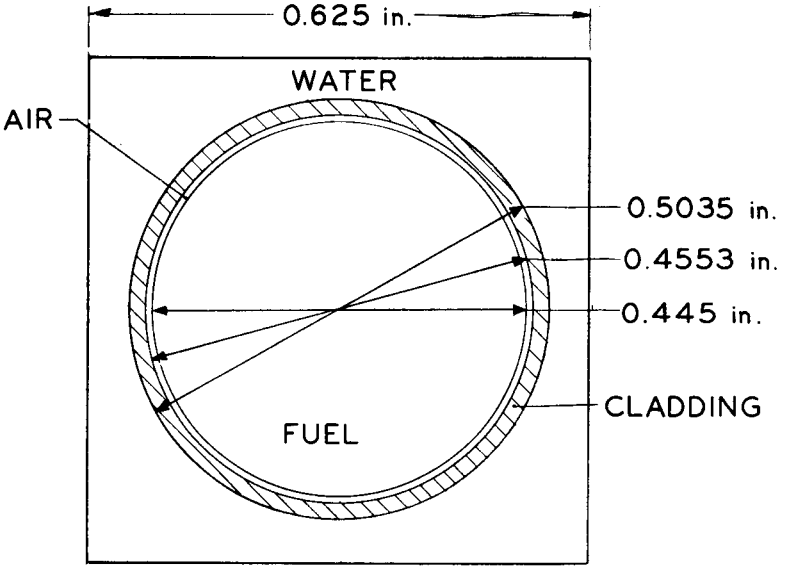

Boiler Unit Fuel Cell

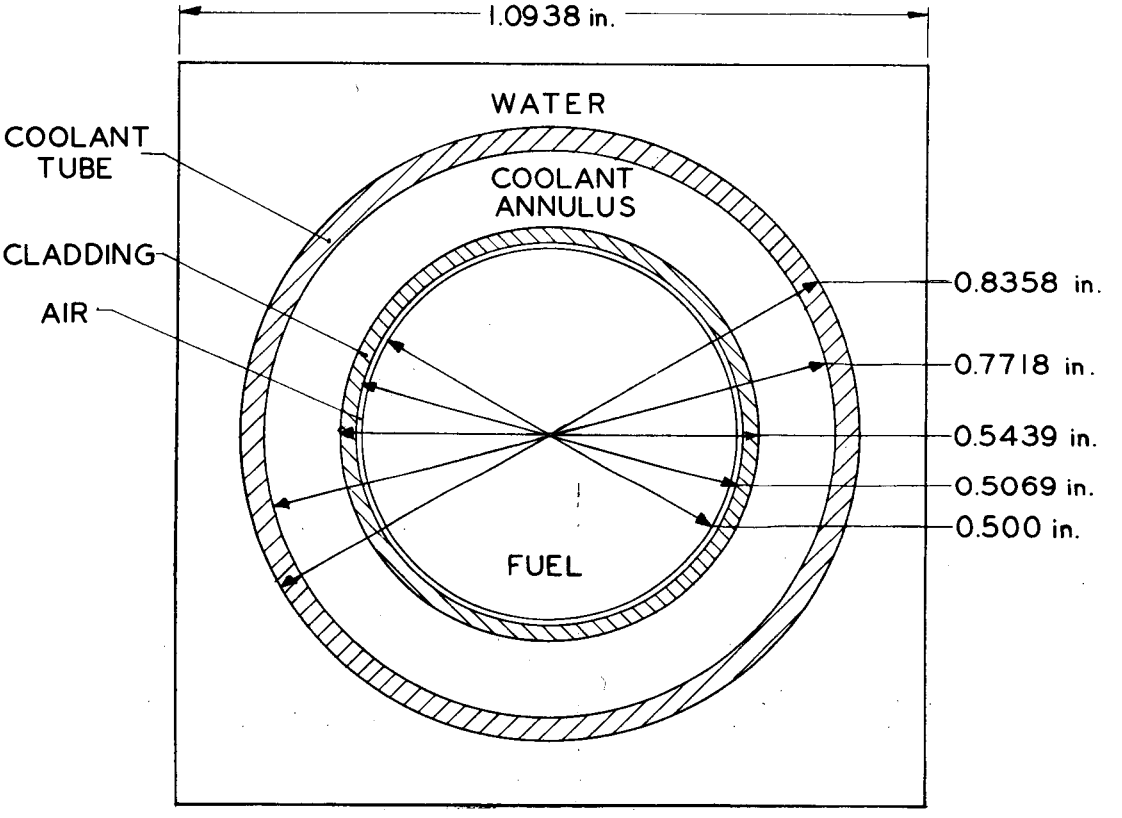

Superheater Unit Fuel Cell

Figure 2. Dimensions of the Boiler and Superheater Unit Cells

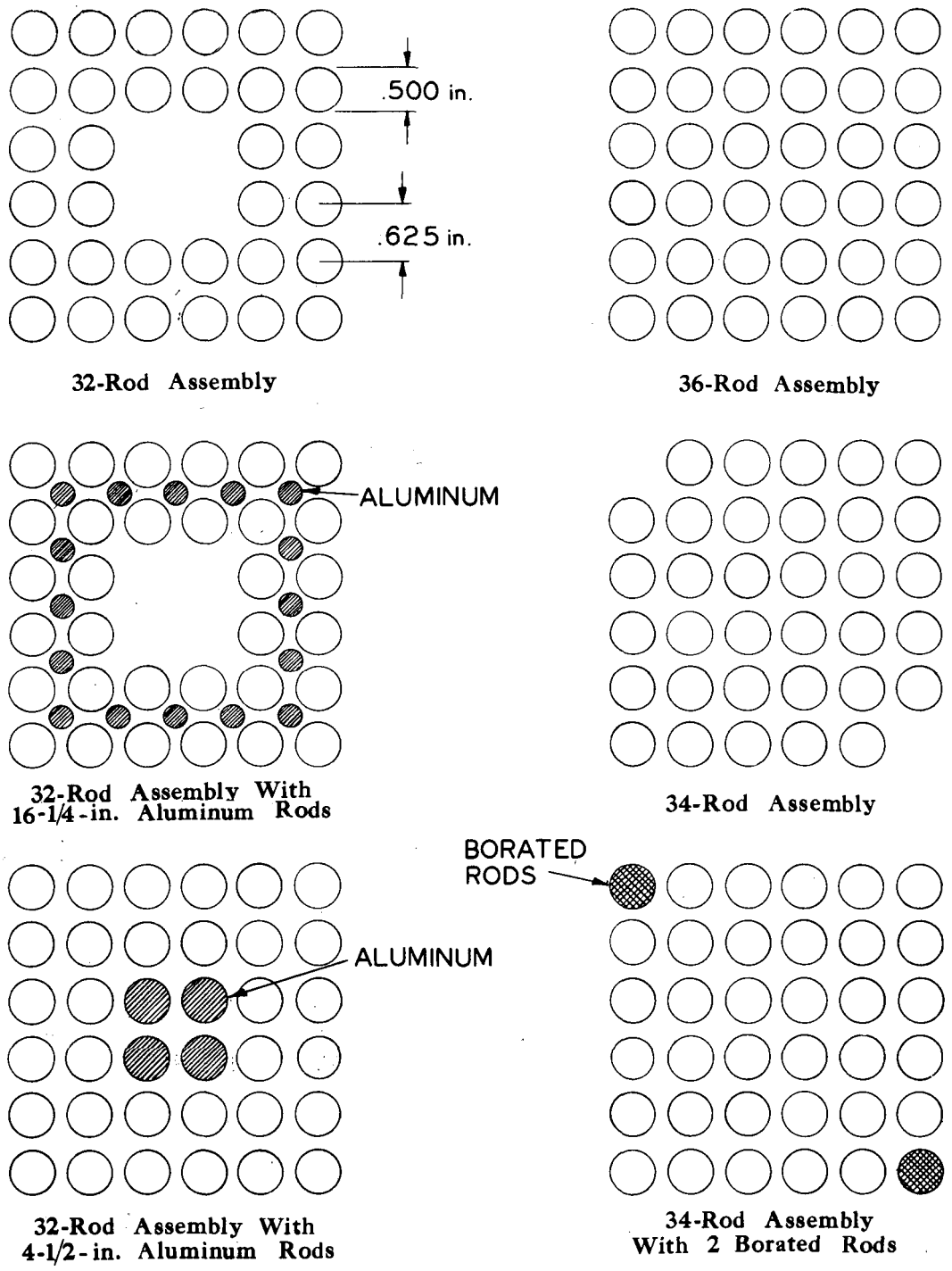

Figure 3. Arrangements of Fuel Rods and Other Materials Within the Boiler Fuel Assemblies

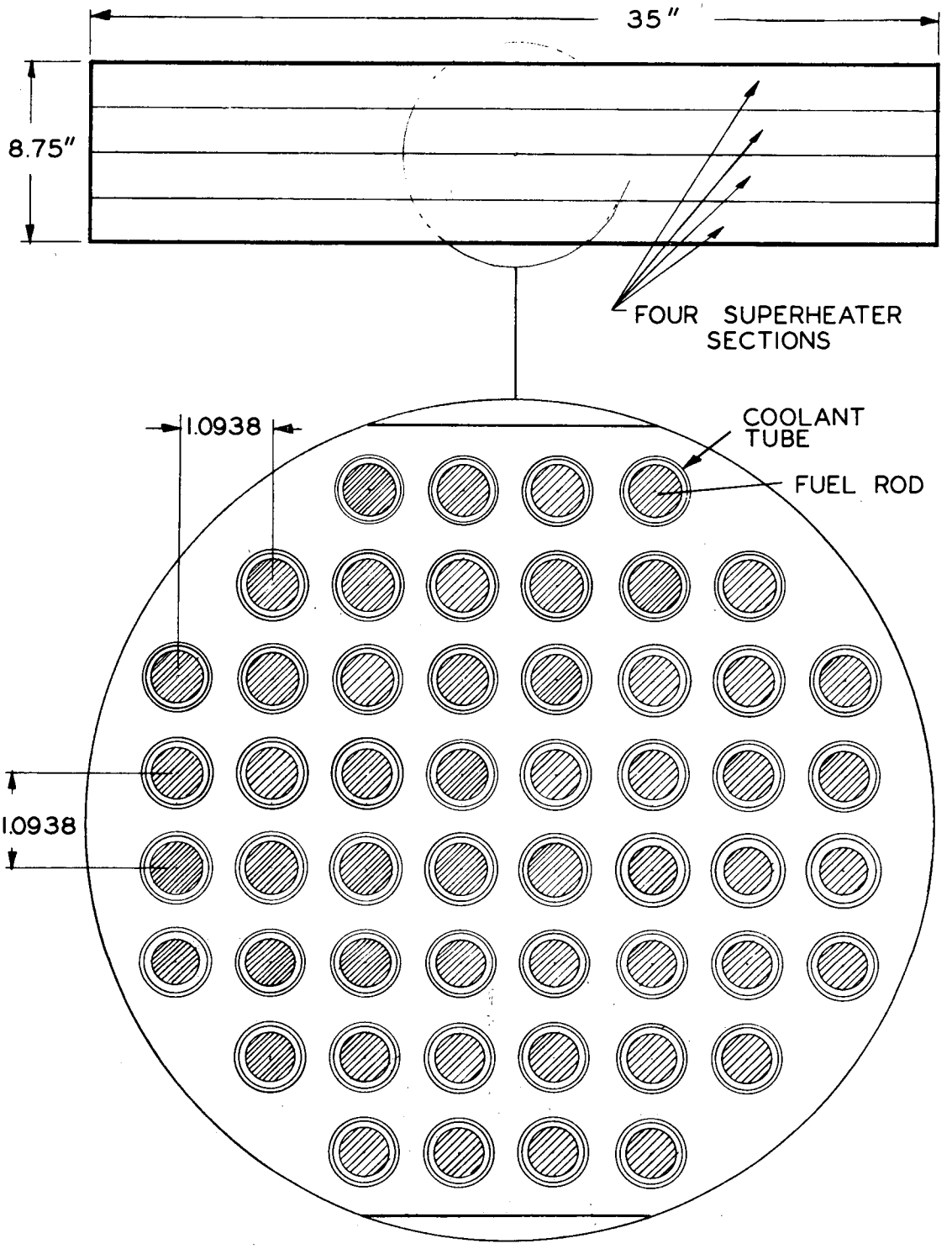

Figure 4. Arrangement of the Superheater Region

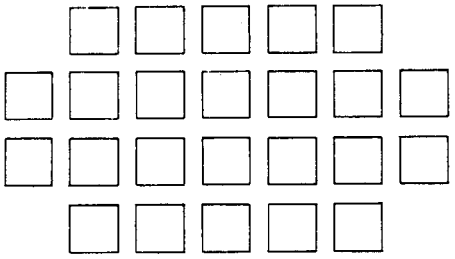

20-Assembly Core

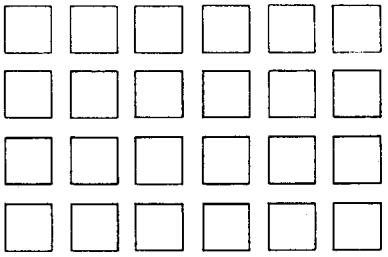

24-Assembly Core

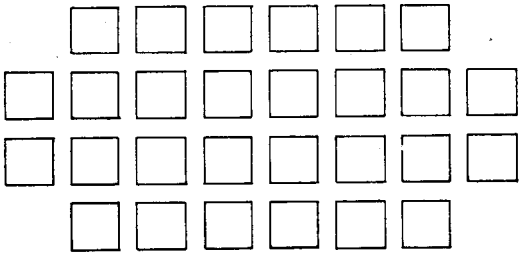

28-Assembly Core

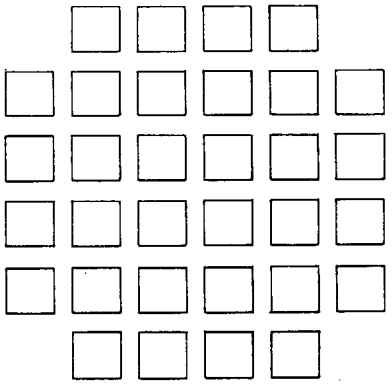

32-Assembly Core

Figure 5. Arrangement of the Boiler Fuel Assemblies

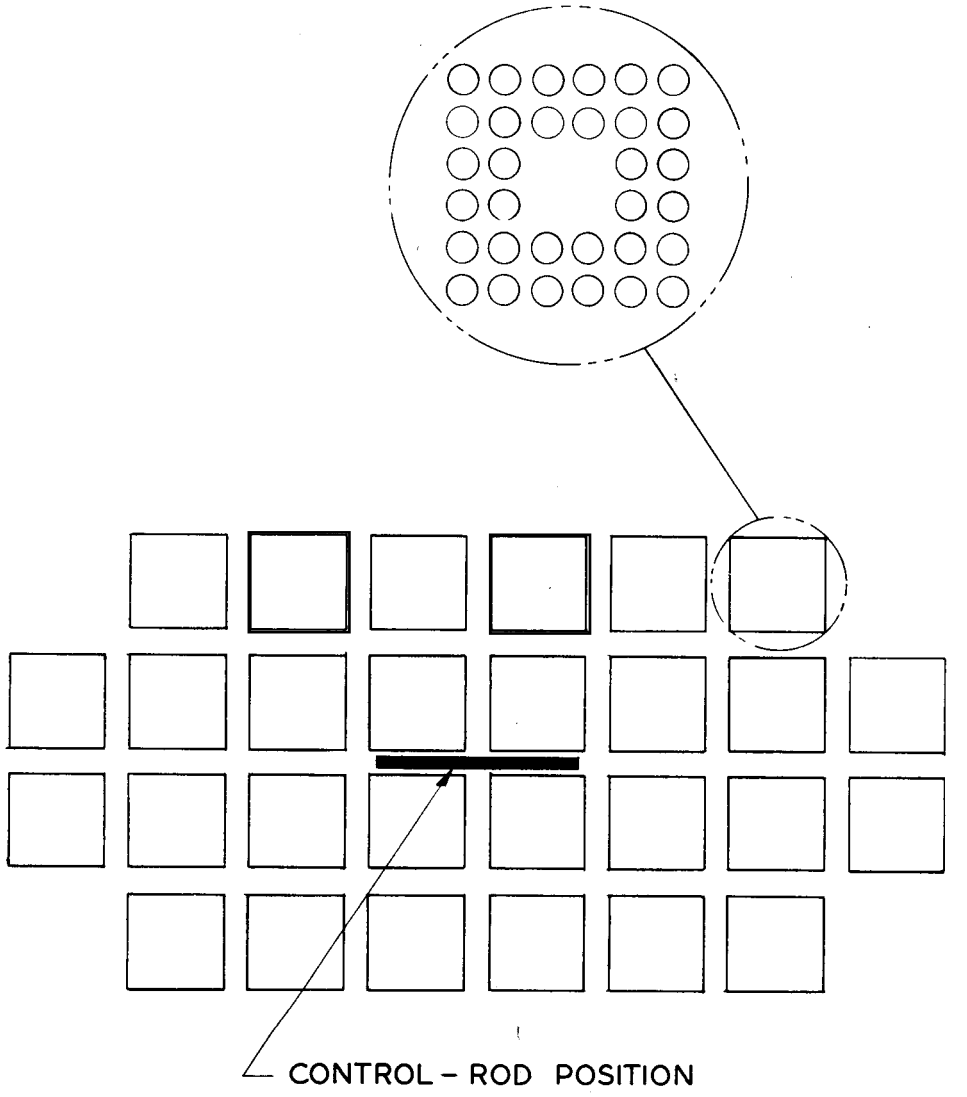

Figure 6. Arrangement of the Boiler Fuel Assemblies for Control-Rod Evaluation

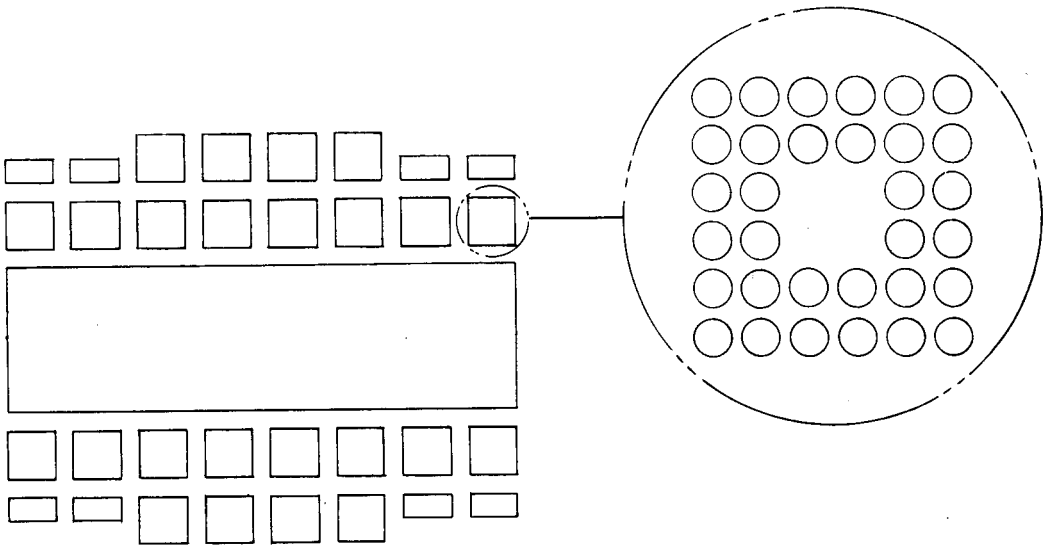

Internal Superheater

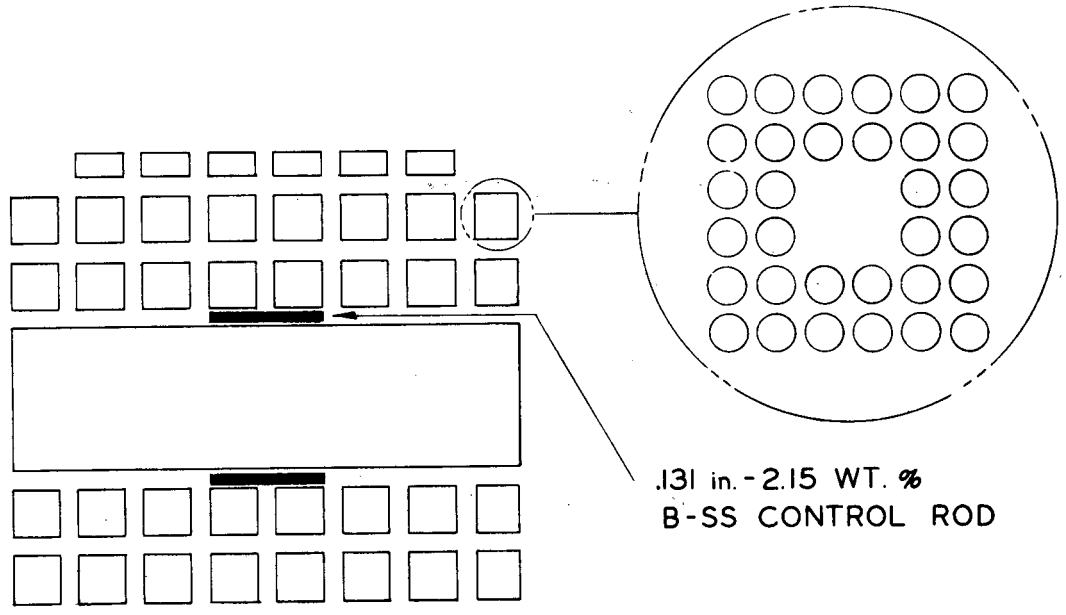

Internal Superheater With Control Rod

Figure 7. Arrangements of Internal Superheater Region With Respect to the Boiler Region

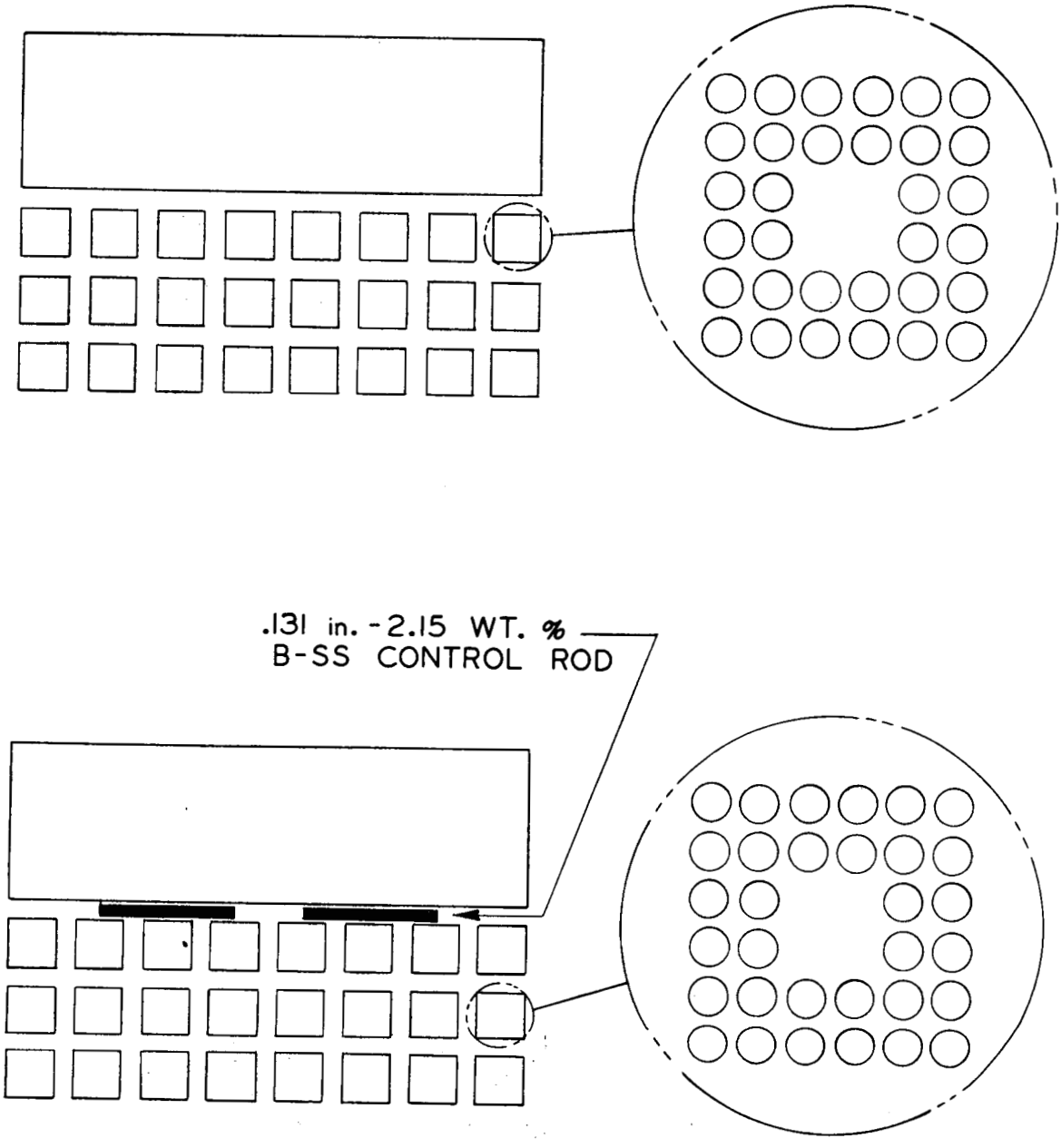

Figure 8. Arrangements of External Superheater Region With Respect to the Boiler Region

2.03* 1.97	1.69	1.65* 1.63	1.60	1.62	1.86* 1.84
1.68	1.50* 1.49	1.55	1.53* 1.53	1.42* 1.43	1.57
1.63* 1.60	1.53			1.47* 1.47	1.50
1.56	1.50* 1.49			1.43	1.43* 1.46
1.55	1.37* 1.37	1.44* 1.43	1.41	1.30* 1.31	1.44
1.76* 1.71	1.47	1.42	1.38* 1.40	1.41	1.61* 1.60

1.75	1.45	1.34	1.28	1.24	1.38* 1.35
1.49	1.27	1.28	1.22	1.09	1.16
1.42	1.31			1.13	1.10
1.38	1.27			1.10	1.07
1.37	1.17	1.18	1.12	1.00	1.06
1.54* 1.52	1.26	1.17	1.11	1.08	1.20* 1.18

1.21* 1.18	0.94	0.82	0.74	0.70	0.77* 0.79
1.01	0.82	0.78	0.70	0.62	0.69
0.96	0.84			0.64	0.67
0.93	0.82			0.63	0.65
0.93	0.75	0.72	0.65	0.57	0.64
1.02* 1.03	0.82	0.71	0.64	0.61	0.65* 0.69

1.53* 1.54	1.32	1.26	1.25	1.26	1.47* 1.43
1.23	1.08	1.12	1.11	1.04	1.15
1.09	1.04			1.00	1.02
0.99	0.95			0.91	0.92
0.94	0.84	0.88	0.87	0.81	0.88
1.03* 1.08	0.95	0.93	0.91	0.92	0.97* 1.01

1.40* 1.36	1.13	1.04	1.00	0.97	1.10* 1.05
1.09	0.93	0.93	0.88	0.80	0.85
0.96	0.89			0.77	0.75
0.87	0.81			0.70	0.68
0.83	0.72	0.73	0.70	0.62	0.65
0.90* 0.95	0.82	0.77	0.73	0.70	0.71* 0.74

0.95* 0.93	0.73	0.64* 0.64	0.57	0.54	0.59* 0.61
0.74	0.60* 0.60	0.56	0.52* 0.51	0.45* 0.45	0.51
0.66* 0.65	0.57			0.43* 0.44	0.45
0.59	0.53* 0.52			0.40	0.39* 0.41
0.57	0.46* 0.47	0.43* 0.44	0.40	0.34* 0.35	0.39
0.61* 0.65	0.53	0.47	0.40* 0.42	0.39	0.39* 0.42

• Experimental measurement.

Figure 9. Rod-By-Rod Power Distributions for One Quadrant of a 24-Assembly Core With 32 Fuel Rods per Assembly (Average Rod Power Normalized to Unity)

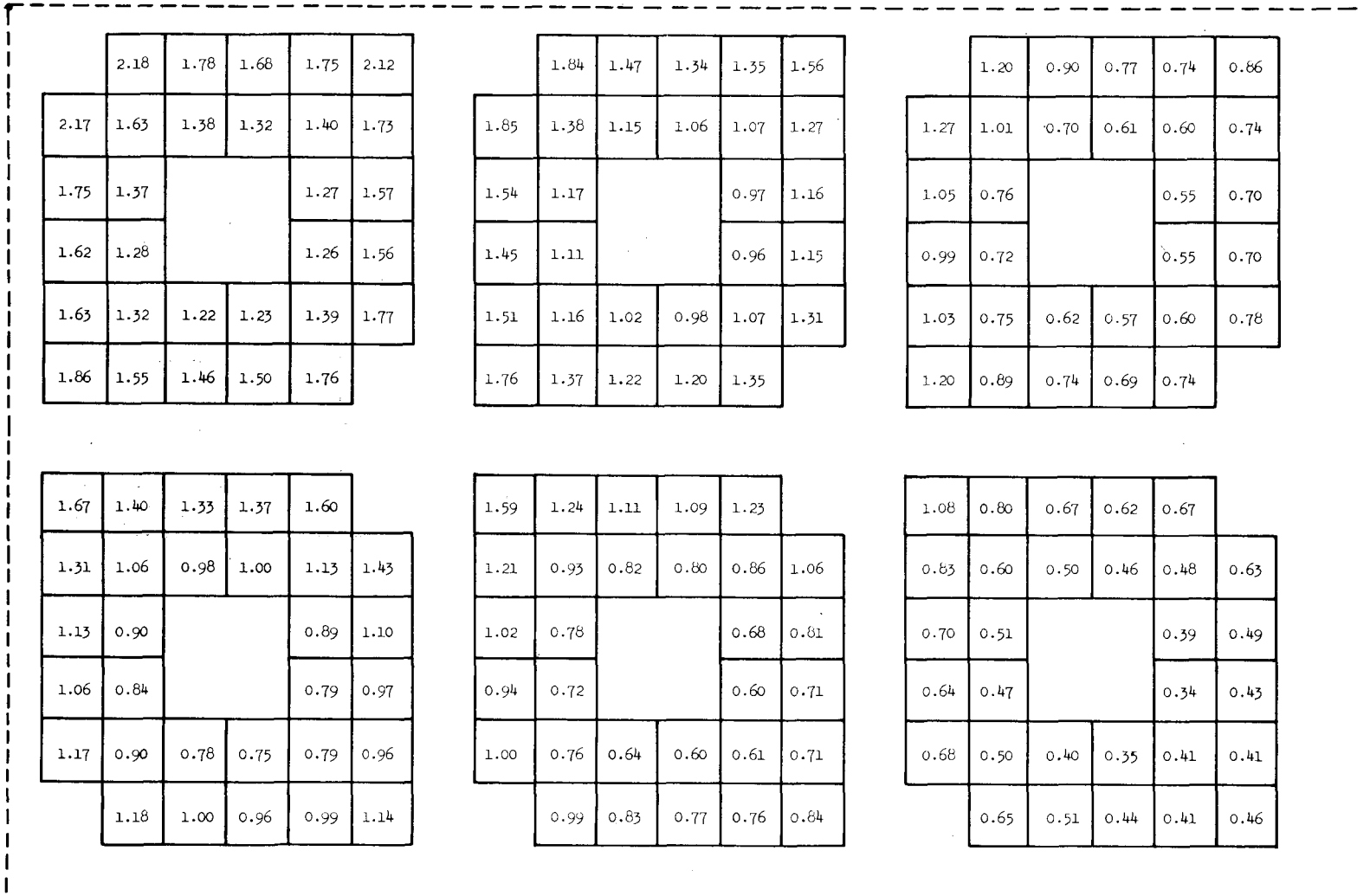

	2.18	1.78	1.68	1.75	2.12
2.17	1.63	1.38	1.32	1.40	1.73
1.75	1.37			1.27	1.57
1.62	1.28			1.26	1.56
1.63	1.32	1.22	1.23	1.39	1.77
1.86	1.55	1.46	1.50	1.76	

	1.84	1.47	1.34	1.35	1.56
1.85	1.38	1.15	1.06	1.07	1.27
1.54	1.17			0.97	1.16
1.45	1.11			0.96	1.15
1.51	1.16	1.02	0.98	1.07	1.31
1.76	1.37	1.22	1.20	1.35	

	1.20	0.90	0.77	0.74	0.86
1.27	1.01	0.70	0.61	0.60	0.74
1.05	0.76			0.55	0.70
0.99	0.72			0.55	0.70
1.03	0.75	0.62	0.57	0.60	0.78
1.20	0.89	0.74	0.69	0.74	

1.67	1.40	1.33	1.37	1.60	
1.31	1.06	0.98	1.00	1.13	1.43
1.13	0.90			0.89	1.10
1.06	0.84			0.79	0.97
1.17	0.90	0.78	0.75	0.79	0.96
	1.18	1.00	0.96	0.99	1.14

1.59	1.24	1.11	1.09	1.23	
1.21	0.93	0.82	0.80	0.86	1.06
1.02	0.78			0.68	0.81
0.94	0.72			0.60	0.71
1.00	0.76	0.64	0.60	0.61	0.71
	0.99	0.83	0.77	0.76	0.84

1.08	0.80	0.67	0.62	0.67	
0.83	0.60	0.50	0.46	0.48	0.63
0.70	0.51			0.39	0.49
0.64	0.47			0.34	0.43
0.68	0.50	0.40	0.35	0.41	0.41
	0.65	0.51	0.44	0.41	0.46

Figure 10. Rod-By-Rod Power Distributions for One Quadrant of a 24-Assembly Core With 34 Fuel Rods per Assembly (Average Rod Power Normalized to Unity)

2.34* 2.22	1.86	1.72	1.70	1.78	2.08* 2.07
1.87* 1.84	1.49	1.36	1.34	1.42	1.72
1.77* 1.70	1.35* 1.35	1.21* 1.23	1.21	1.29	1.58
1.65	1.31	1.19	1.17* 1.18	1.25	1.53
1.69	1.36	1.25	1.21* 1.23	1.30	1.57
1.95* 1.93	1.61	1.49	1.47* 1.47	1.51* 1.54	1.83* 1.80

1.94* 1.97	1.59	1.43	1.36	1.36	1.53
1.62* 1.64	1.28	1.13	1.07	1.09	1.27
1.48* 1.51	1.17* 1.16	1.04* 1.02	0.97	0.99	1.16
1.46	1.13	0.99	0.94	0.96	1.13
1.50	1.17	1.03	0.98	1.00	1.16
1.71	1.38	1.24	1.17	1.18	1.30* 1.32

1.36* 1.34	1.03	0.87	0.78	0.76	0.89
1.09* 1.12	0.83	0.69	0.62	0.62	0.76
1.03* 1.03	0.74* 0.75	0.62* 0.62	0.56	0.56	0.71
1.00	0.73	0.61	0.54	0.55	0.69
1.02	0.76	0.63	0.57	0.56	0.70
1.16	0.89	0.75	0.67	0.66	0.73* 0.77

1.69* 1.73	1.45	1.35	1.33	1.39	1.62
1.37* 1.35	1.09	1.00	0.99	1.04	1.26
1.15* 1.15	0.92* 0.92	0.86* 0.84	0.83	0.88	1.07
1.04	0.84	0.76	0.75	0.80	0.97
1.03	0.84	0.77	0.76	0.80	0.96
1.21	1.05	0.98	0.97	1.00	1.09* 1.13

1.56* 1.54	1.25	1.12	1.06	1.06	1.19
1.22* 1.20	0.94	0.83	0.79	0.80	0.93
1.02* 1.02	0.82* 0.79	0.71* 0.70	0.66	0.67	0.79
0.93	0.72	0.63	0.60	0.61	0.72
0.91	0.72	0.64	0.61	0.62	0.71
1.07	0.90	0.82	0.78	0.77	0.79* 0.84

1.03* 1.05	0.81	0.68	0.61	0.59	0.69
0.80* 0.82	0.61	0.51	0.46	0.45	0.56
0.71* 0.70	0.52* 0.51	0.43* 0.43	0.38	0.38	0.48
0.63	0.47	0.39	0.35	0.35	0.44
0.62	0.47	0.39	0.35	0.35	0.42
0.73	0.58	0.50	0.45	0.42	0.43* 0.47

* Experimental measurement.

Figure 11. Rod-By-Rod Power Distributions for One Quadrant of a 24-Assembly Core With 36 Fuel Rods per Assembly (Average Rod Power Normalized to Unity)

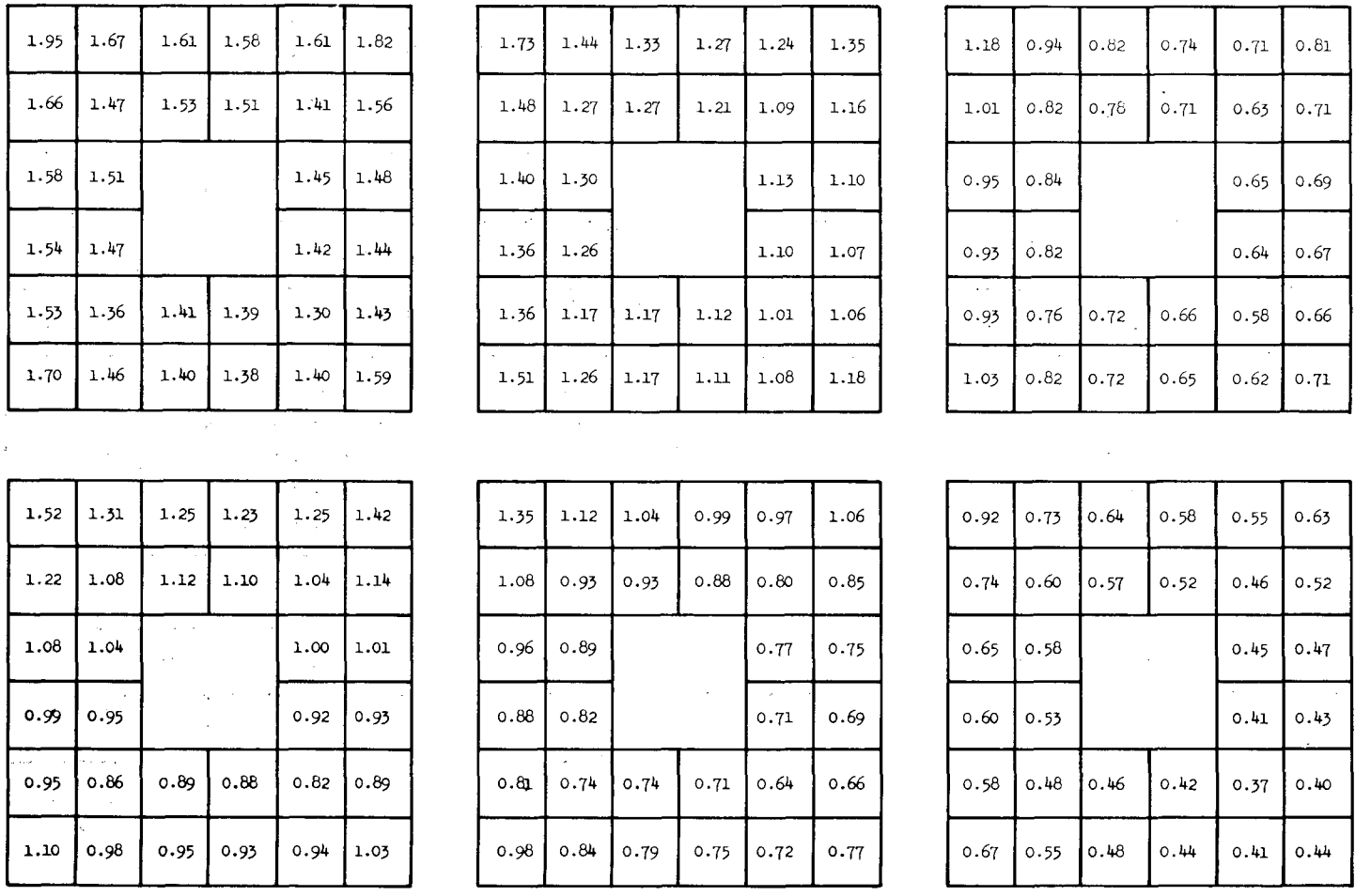

1.95	1.67	1.61	1.58	1.61	1.82
1.66	1.47	1.53	1.51	1.41	1.56
1.58	1.51			1.45	1.48
1.54	1.47			1.42	1.44
1.53	1.36	1.41	1.39	1.30	1.43
1.70	1.46	1.40	1.38	1.40	1.59

1.73	1.44	1.33	1.27	1.24	1.35
1.48	1.27	1.27	1.21	1.09	1.16
1.40	1.30			1.13	1.10
1.36	1.26			1.10	1.07
1.36	1.17	1.17	1.12	1.01	1.06
1.51	1.26	1.17	1.11	1.08	1.18

1.18	0.94	0.82	0.74	0.71	0.81
1.01	0.82	0.78	0.71	0.63	0.71
0.95	0.84			0.65	0.69
0.93	0.82			0.64	0.67
0.93	0.76	0.72	0.66	0.58	0.66
1.03	0.82	0.72	0.65	0.62	0.71

1.52	1.31	1.25	1.23	1.25	1.42
1.22	1.08	1.12	1.10	1.04	1.14
1.08	1.04			1.00	1.01
0.99	0.95			0.92	0.93
0.95	0.86	0.89	0.88	0.82	0.89
1.10	0.98	0.95	0.93	0.94	1.03

1.35	1.12	1.04	0.99	0.97	1.06
1.08	0.93	0.93	0.88	0.80	0.85
0.96	0.89			0.77	0.75
0.88	0.82			0.71	0.69
0.81	0.74	0.74	0.71	0.64	0.66
0.98	0.84	0.79	0.75	0.72	0.77

0.92	0.73	0.64	0.58	0.55	0.63
0.74	0.60	0.57	0.52	0.46	0.52
0.65	0.58			0.45	0.47
0.60	0.53			0.41	0.43
0.58	0.48	0.46	0.42	0.37	0.40
0.67	0.55	0.48	0.44	0.41	0.44

Figure 12. Rod-By-Rod Power Distributions for One Quadrant of a 24-Assembly Core With 32 Fuel Rods and 16—1/4-in. Aluminum Rods per Assembly (Average Rod Power Normalized to Unity)

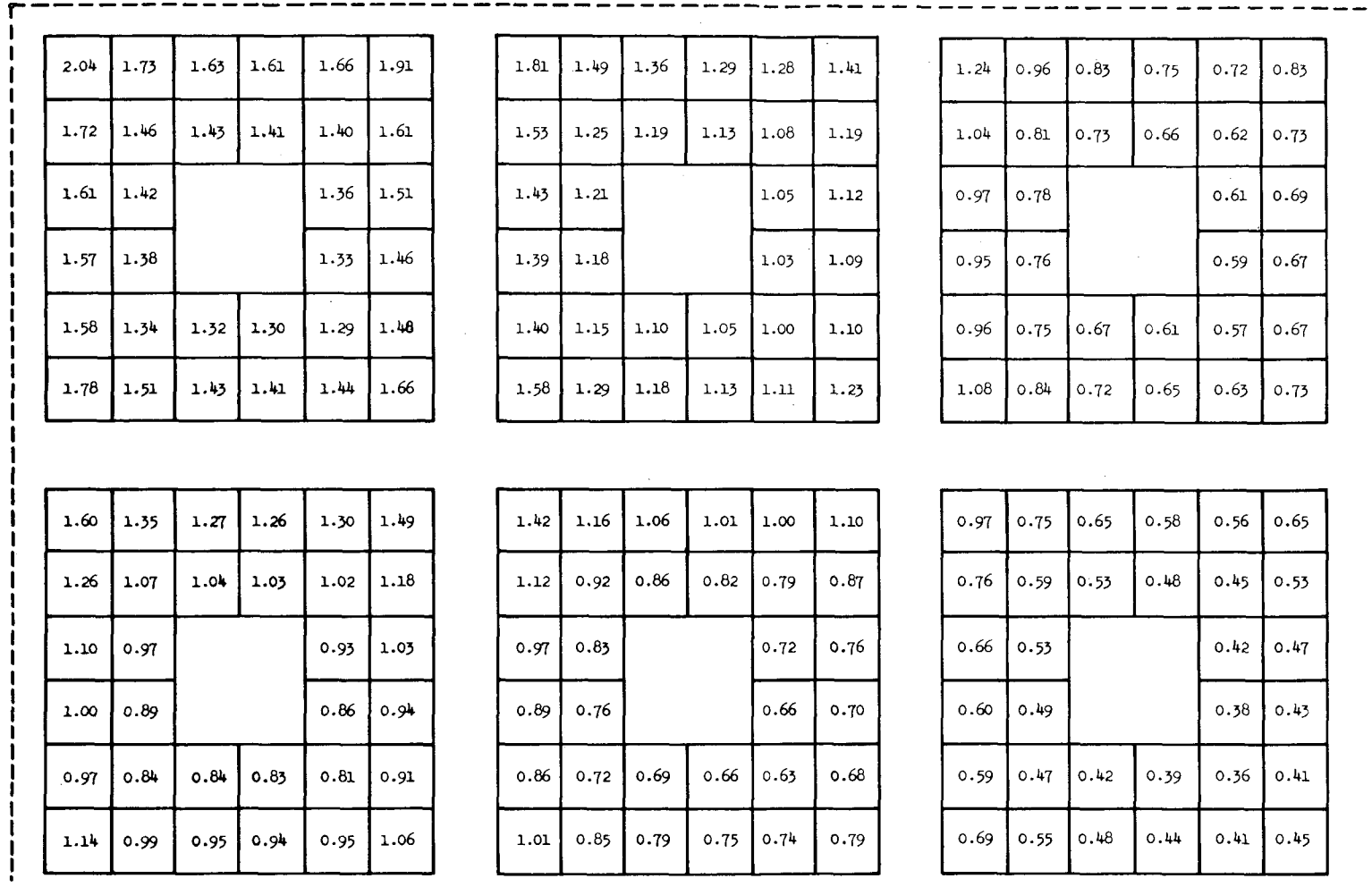

2.04	1.73	1.63	1.61	1.66	1.91
1.72	1.46	1.43	1.41	1.40	1.61
1.61	1.42			1.36	1.51
1.57	1.38			1.33	1.46
1.58	1.34	1.32	1.30	1.29	1.48
1.78	1.51	1.43	1.41	1.44	1.66

1.81	1.49	1.36	1.29	1.28	1.41
1.53	1.25	1.19	1.13	1.08	1.19
1.43	1.21			1.05	1.12
1.39	1.18			1.03	1.09
1.40	1.15	1.10	1.05	1.00	1.10
1.58	1.29	1.18	1.13	1.11	1.23

1.24	0.96	0.83	0.75	0.72	0.83
1.04	0.81	0.73	0.66	0.62	0.73
0.97	0.78			0.61	0.69
0.95	0.76			0.59	0.67
0.96	0.75	0.67	0.61	0.57	0.67
1.08	0.84	0.72	0.65	0.63	0.73

1.60	1.35	1.27	1.26	1.30	1.49
1.26	1.07	1.04	1.03	1.02	1.18
1.10	0.97			0.93	1.03
1.00	0.89			0.86	0.94
0.97	0.84	0.84	0.83	0.81	0.91
1.14	0.99	0.95	0.94	0.95	1.06

1.42	1.16	1.06	1.01	1.00	1.10
1.12	0.92	0.86	0.82	0.79	0.87
0.97	0.83			0.72	0.76
0.89	0.76			0.66	0.70
0.86	0.72	0.69	0.66	0.63	0.68
1.01	0.85	0.79	0.75	0.74	0.79

0.97	0.75	0.65	0.58	0.56	0.65
0.76	0.59	0.53	0.48	0.45	0.53
0.66	0.53			0.42	0.47
0.60	0.49			0.38	0.43
0.59	0.47	0.42	0.39	0.36	0.41
0.69	0.55	0.48	0.44	0.41	0.45

Figure 13. Rod-By-Rod Power Distributions for One Quadrant of a 24-Assembly Core With 32 Fuel Rods and 4—1/2-in. Aluminum Rods per Assembly (Average Rod Power Normalized to Unity)

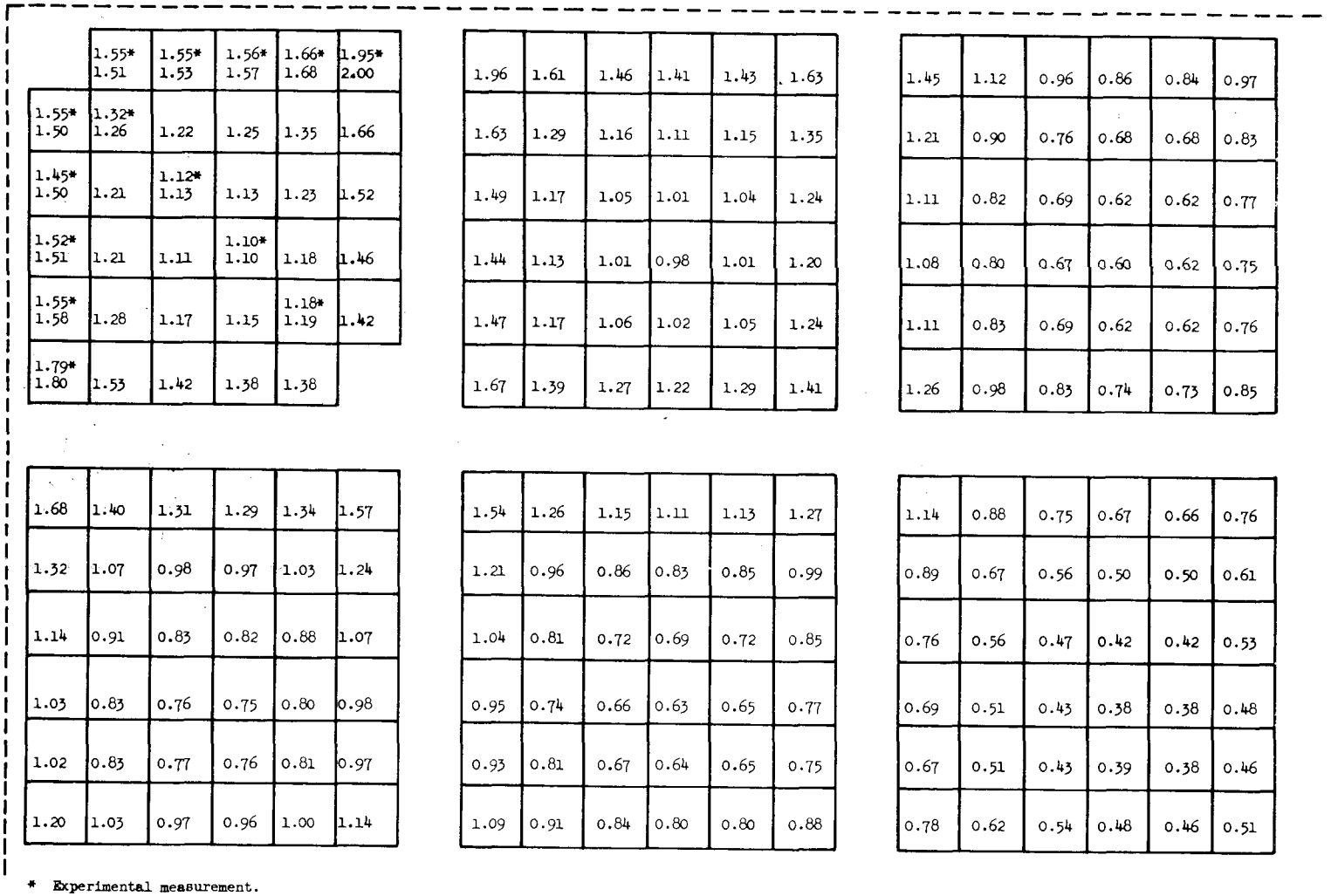

	1.55* 1.51	1.55* 1.53	1.56* 1.57	1.66* 1.68	1.95* 2.00
1.55* 1.50	1.32* 1.26	1.22	1.25	1.35	1.66
1.45* 1.50	1.21	1.12* 1.13	1.13	1.23	1.52
1.52* 1.51	1.21	1.11	1.10* 1.10	1.18	1.46
1.55* 1.58	1.28	1.17	1.15	1.18* 1.19	1.42
1.79* 1.80	1.53	1.42	1.38	1.38	

1.96	1.61	1.46	1.41	1.43	1.63
1.63	1.29	1.16	1.11	1.15	1.35
1.49	1.17	1.05	1.01	1.04	1.24
1.44	1.13	1.01	0.98	1.01	1.20
1.47	1.17	1.06	1.02	1.05	1.24
1.67	1.39	1.27	1.22	1.29	1.41

1.45	1.12	0.96	0.86	0.84	0.97
1.21	0.90	0.76	0.68	0.68	0.83
1.11	0.82	0.69	0.62	0.62	0.77
1.08	0.80	0.67	0.60	0.62	0.75
1.11	0.83	0.69	0.62	0.62	0.76
1.26	0.98	0.83	0.74	0.73	0.85

1.68	1.40	1.31	1.29	1.34	1.57
1.32	1.07	0.98	0.97	1.03	1.24
1.14	0.91	0.83	0.82	0.88	1.07
1.03	0.83	0.76	0.75	0.80	0.98
1.02	0.83	0.77	0.76	0.81	0.97
1.20	1.03	0.97	0.96	1.00	1.14

1.54	1.26	1.15	1.11	1.13	1.27
1.21	0.96	0.86	0.83	0.85	0.99
1.04	0.81	0.72	0.69	0.72	0.85
0.95	0.74	0.66	0.63	0.65	0.77
0.93	0.81	0.67	0.64	0.65	0.75
1.09	0.91	0.84	0.80	0.80	0.88

1.14	0.88	0.75	0.67	0.66	0.76
0.89	0.67	0.56	0.50	0.50	0.61
0.76	0.56	0.47	0.42	0.42	0.53
0.69	0.51	0.43	0.38	0.38	0.48
0.67	0.51	0.43	0.39	0.38	0.46
0.78	0.62	0.54	0.48	0.46	0.51

* Experimental measurement.

Figure 14. Rod-By-Rod Power Distributions for One Quadrant of a 24-Assembly Core With 36 Fuel Rods per Assembly and Two Pyrex-Boron Rods in the Corners of the Central Four Assemblies (Average Rod Power Normalized to Unity)

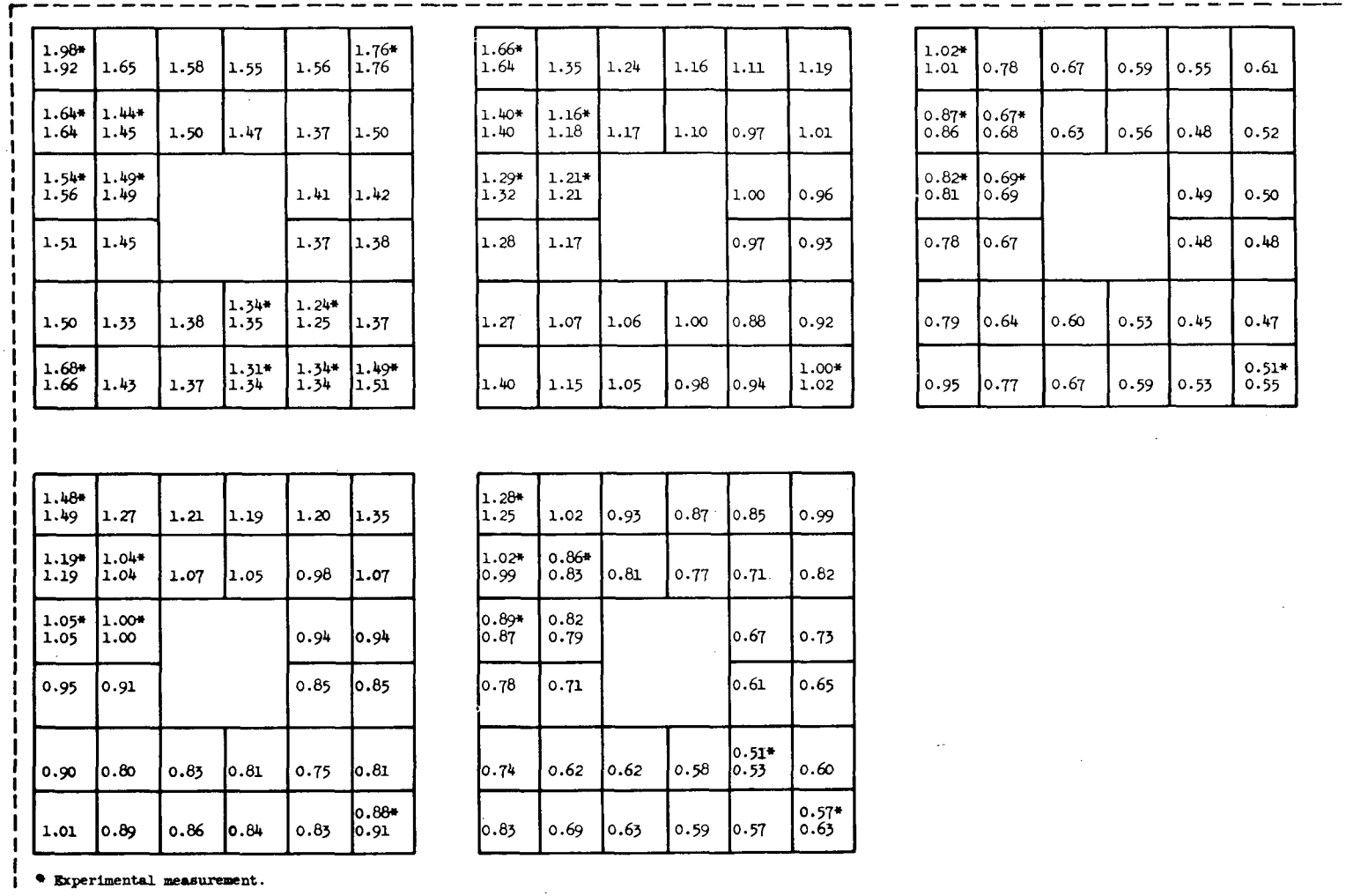

1.98* 1.92	1.65	1.58	1.55	1.56	1.76* 1.76
1.64* 1.64	1.44* 1.45	1.50	1.47	1.37	1.50
1.54* 1.56	1.49* 1.49			1.41	1.42
1.51	1.45			1.37	1.38
1.50	1.33	1.38	1.34* 1.35	1.24* 1.25	1.37
1.68* 1.66	1.43	1.37	1.31* 1.34	1.34* 1.34	1.49* 1.51

1.66* 1.64	1.35	1.24	1.16	1.11	1.19
1.40* 1.40	1.16* 1.18	1.17	1.10	0.97	1.01
1.29* 1.32	1.21* 1.21			1.00	0.96
1.28	1.17			0.97	0.93
1.27	1.07	1.06	1.00	0.88	0.92
1.40	1.15	1.05	0.98	0.94	1.00* 1.02

1.02* 1.01	0.78	0.67	0.59	0.55	0.61
0.87* 0.86	0.67* 0.68	0.63	0.56	0.48	0.52
0.82* 0.81	0.69* 0.69			0.49	0.50
0.78	0.67			0.48	0.48
0.79	0.64	0.60	0.53	0.45	0.47
0.95	0.77	0.67	0.59	0.53	0.51* 0.55

1.48* 1.49	1.27	1.21	1.19	1.20	1.35
1.19* 1.19	1.04* 1.04	1.07	1.05	0.98	1.07
1.05* 1.05	1.00* 1.00			0.94	0.94
0.95	0.91			0.85	0.85
0.90	0.80	0.83	0.81	0.75	0.81
1.01	0.89	0.86	0.84	0.83	0.88* 0.91

1.28* 1.25	1.02	0.93	0.87	0.85	0.99
1.02* 0.99	0.86* 0.83	0.81	0.77	0.71	0.82
0.89* 0.87	0.82 0.79			0.67	0.73
0.78	0.71			0.61	0.65
0.74	0.62	0.62	0.58	0.51* 0.53	0.60
0.83	0.69	0.63	0.59	0.57	0.57* 0.63

* Experimental measurement.

Figure 15. Rod-By-Rod Power Distributions for One Quadrant of a 20-Assembly Core With 32 Fuel Rods per Assembly (Average Rod Power Normalized to Unity)

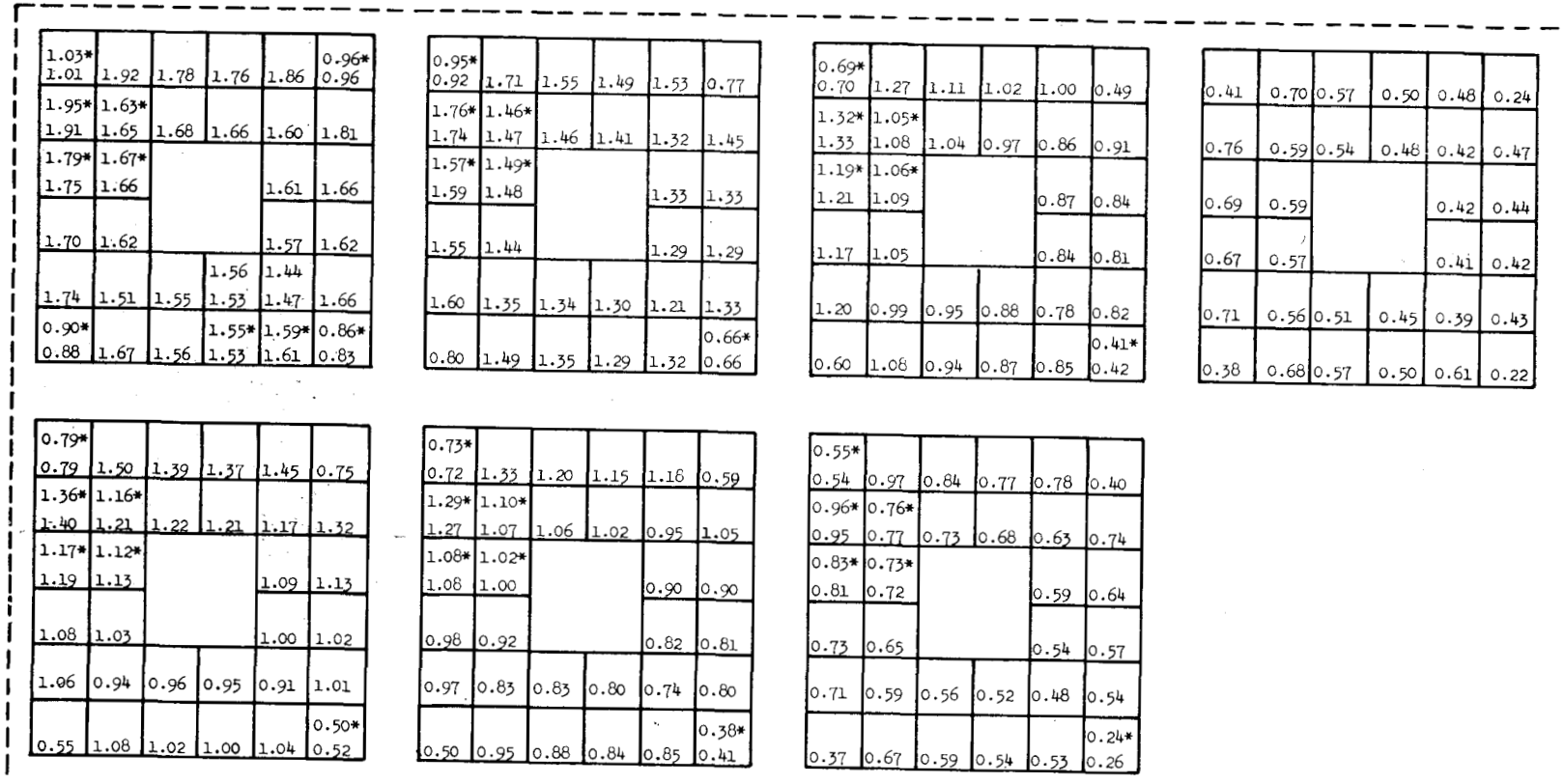

1.03* 1.01	1.92	1.78	1.76	1.86	0.96* 0.96
1.95* 1.91	1.63* 1.65	1.68	1.66	1.60	1.81
1.79* 1.75	1.67* 1.66			1.61	1.66
1.70	1.62			1.57	1.62
1.74	1.51	1.55	1.56 1.53	1.44 1.47	1.66
0.90* 0.88	1.67	1.56	1.55* 1.53	1.59* 1.61	0.86* 0.83

0.95* 0.92	1.71	1.55	1.49	1.53	0.77
1.76* 1.74	1.46* 1.47	1.46	1.41	1.32	1.45
1.57* 1.59	1.49* 1.48			1.33	1.33
1.55	1.44			1.29	1.29
1.60	1.35	1.34	1.30	1.21	1.33
0.80	1.49	1.35	1.29	1.32	0.66* 0.66

0.69* 0.70	1.27	1.11	1.02	1.00	0.49
1.32* 1.33	1.05* 1.08	1.04	0.97	0.86	0.91
1.19* 1.21	1.06* 1.09			0.87	0.84
1.17	1.05			0.84	0.81
1.20	0.99	0.95	0.88	0.78	0.82
0.60	1.08	0.94	0.87	0.85	0.41* 0.42

0.41	0.70	0.57	0.50	0.48	0.24
0.76	0.59	0.54	0.48	0.42	0.47
0.69	0.59			0.42	0.44
0.67	0.57			0.41	0.42
0.71	0.56	0.51	0.45	0.39	0.43
0.38	0.68	0.57	0.50	0.61	0.22

0.79* 0.79	1.50	1.39	1.37	1.45	0.75
1.36* 1.40	1.16* 1.21	1.22	1.21	1.17	1.32
1.17* 1.19	1.12* 1.13			1.09	1.13
1.08	1.03			1.00	1.02
1.06	0.94	0.96	0.95	0.91	1.01
0.55	1.08	1.02	1.00	1.04	0.50* 0.52

0.73* 0.72	1.33	1.20	1.15	1.16	0.59
1.29* 1.27	1.10* 1.07	1.06	1.02	0.95	1.05
1.08* 1.08	1.02* 1.00			0.90	0.90
0.98	0.92			0.82	0.81
0.97	0.83	0.83	0.80	0.74	0.80
0.50	0.95	0.88	0.84	0.85	0.38* 0.41

0.55* 0.54	0.97	0.84	0.77	0.78	0.40
0.96* 0.95	0.76* 0.77	0.73	0.68	0.63	0.74
0.83* 0.81	0.73* 0.72			0.59	0.64
0.73	0.65			0.54	0.57
0.71	0.59	0.56	0.52	0.48	0.54
0.37	0.67	0.59	0.54	0.53	0.24* 0.26

* Experimental measurement.

Figure 16. Rod-By-Rod Power Distributions for One Quadrant of a 28-Assembly Core With 32 Fuel Rods per Assembly and the Corner Rods of Each Assembly Possessing a Natural-Uranium Enrichment (Average Rod Power Normalized to Unity)

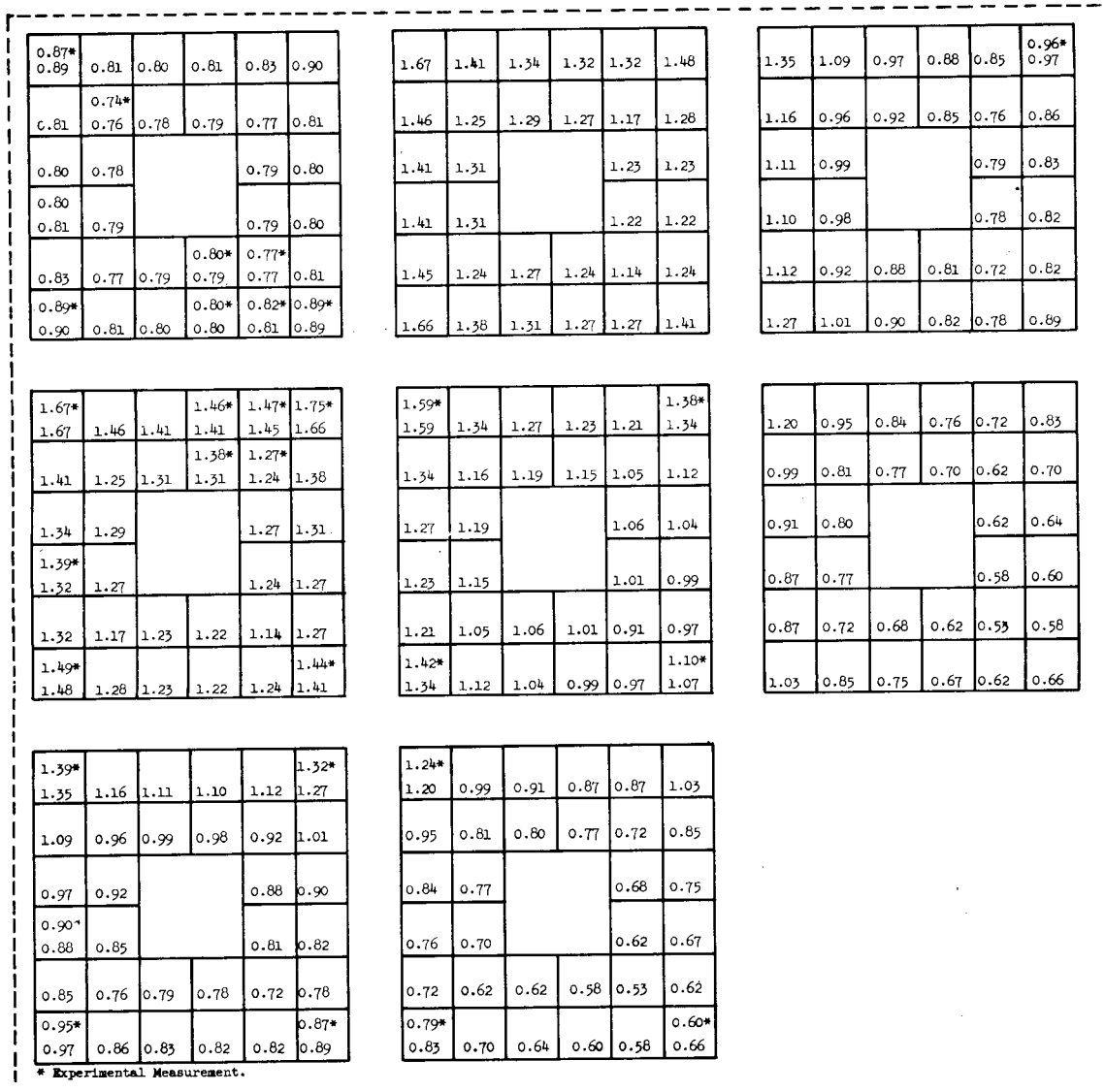

Figure 17. Rod-By-Rod Power Distributions for One Quadrant of a 32-Assembly Core With 32 Fuel Rods per Assembly and the Central Four Assemblies Possessing a Natural-Uranium Enrichment (Average Rod Power Normalized to Unity)

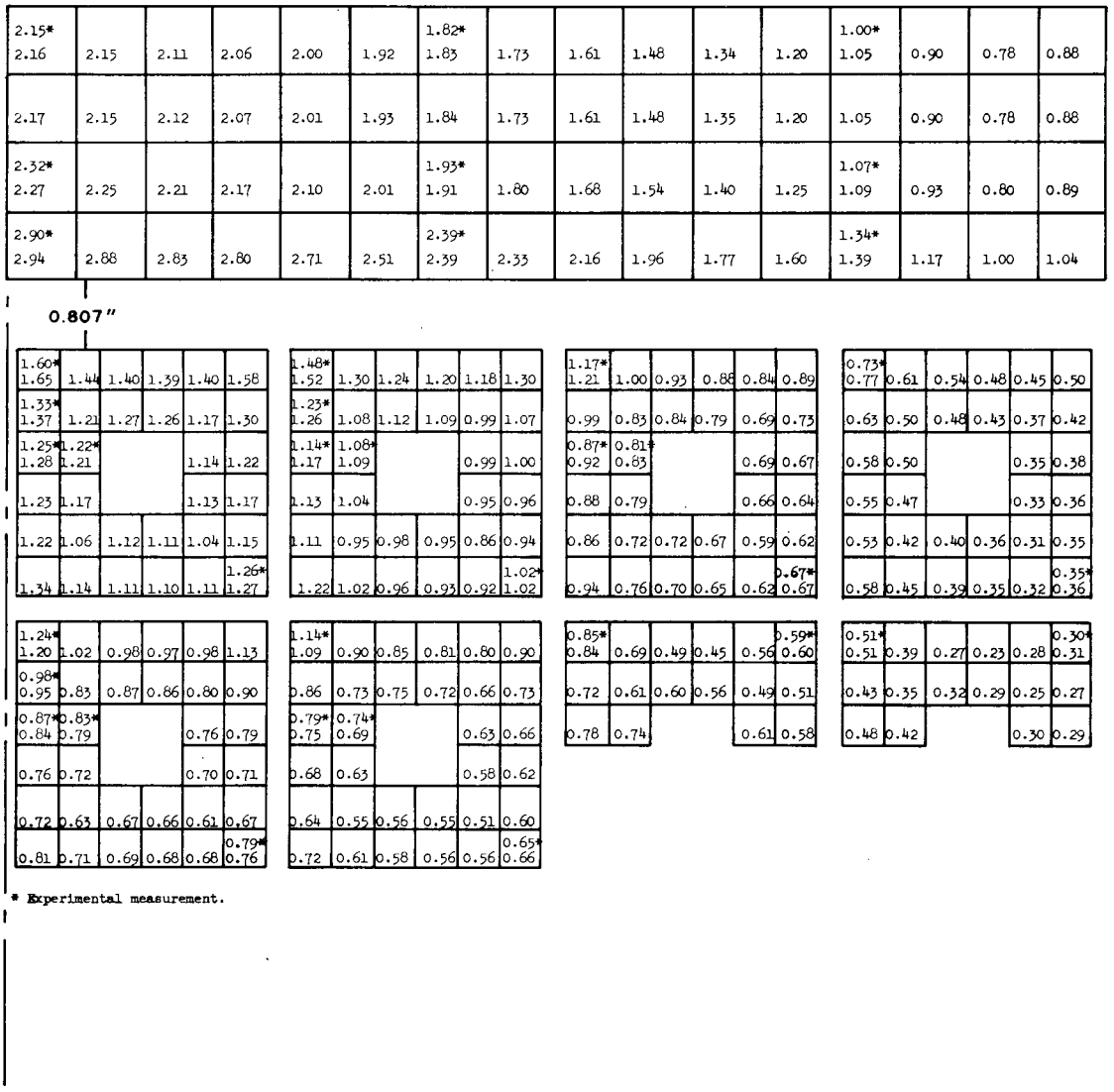

Figure 18. Rod-By-Rod Power Distributions for One Quadrant of the Internal Boiler-Superheater Arrangement With Superheater Voided (Average Rod Power Normalized to Unity)

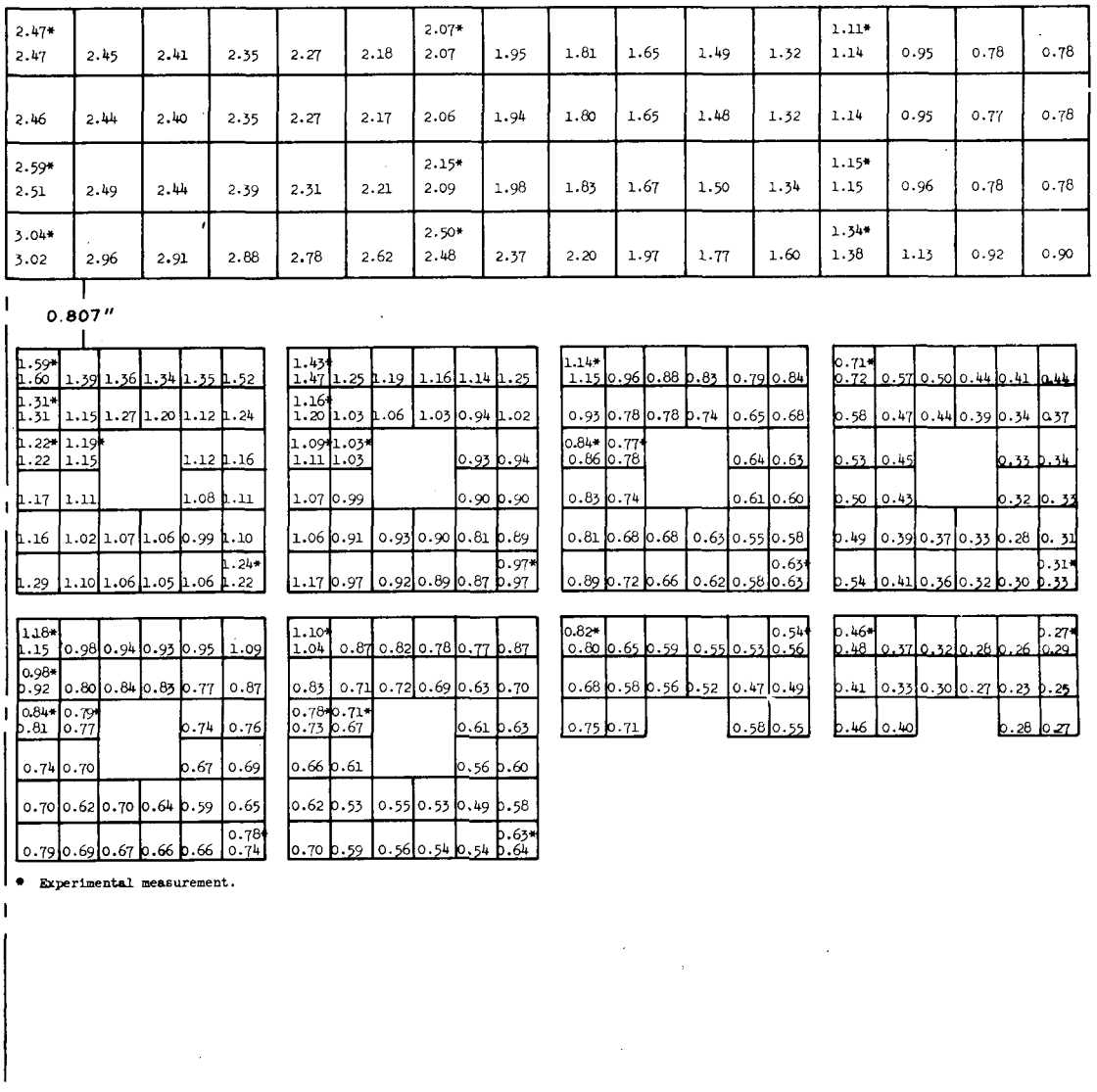

Figure 19. Rod-By-Rod Power Distributions for One Quadrant of the Internal Boiler-Superheater Arrangement With Superheater Flooded (Average Rod Power Normalized to Unity)

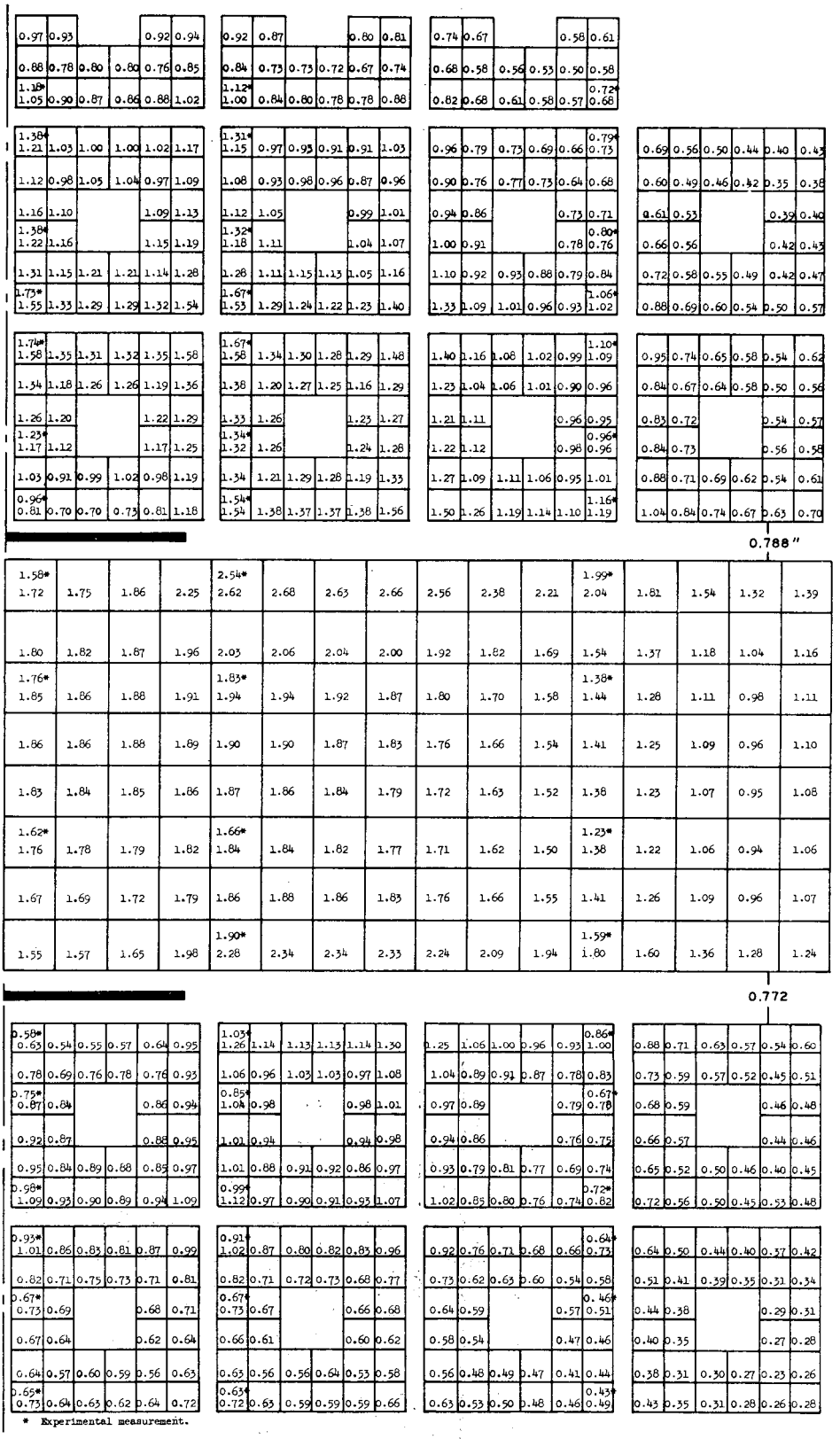

Figure 20. Rod-By-Rod Power Distributions for One-Half of the Internal Boiler-Superheater Arrangement With the Superheater Voided and Two 0.131-in. 2.15 wt.% B-SS Rods Between Regions (Average Rod Power Normalized to Unity)

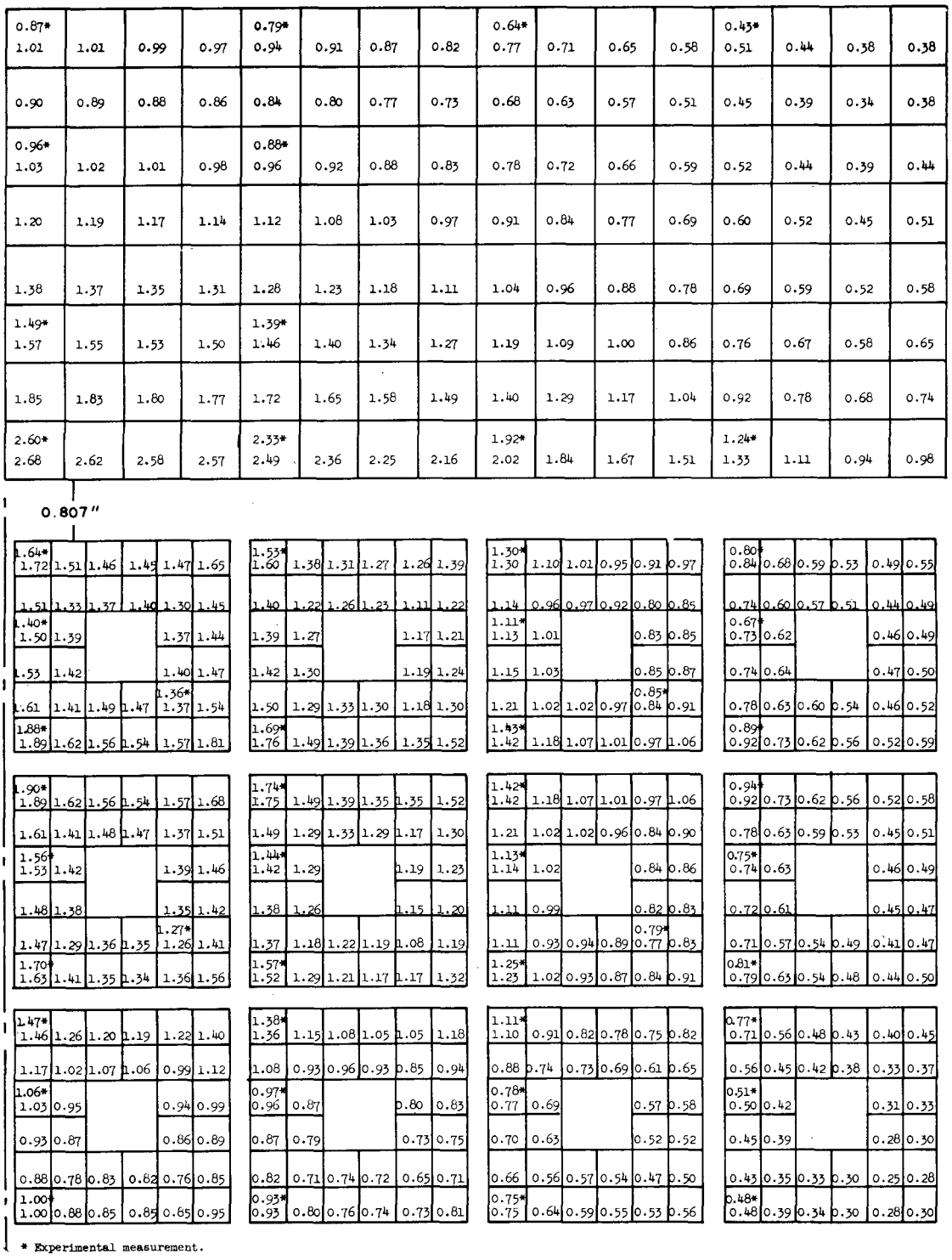

Figure 21. Rod-By-Rod Power Distributions for One-Half of the External Boiler-Superheater Arrangement With Superheater Voided (Average Rod Power Normalized to Unity)

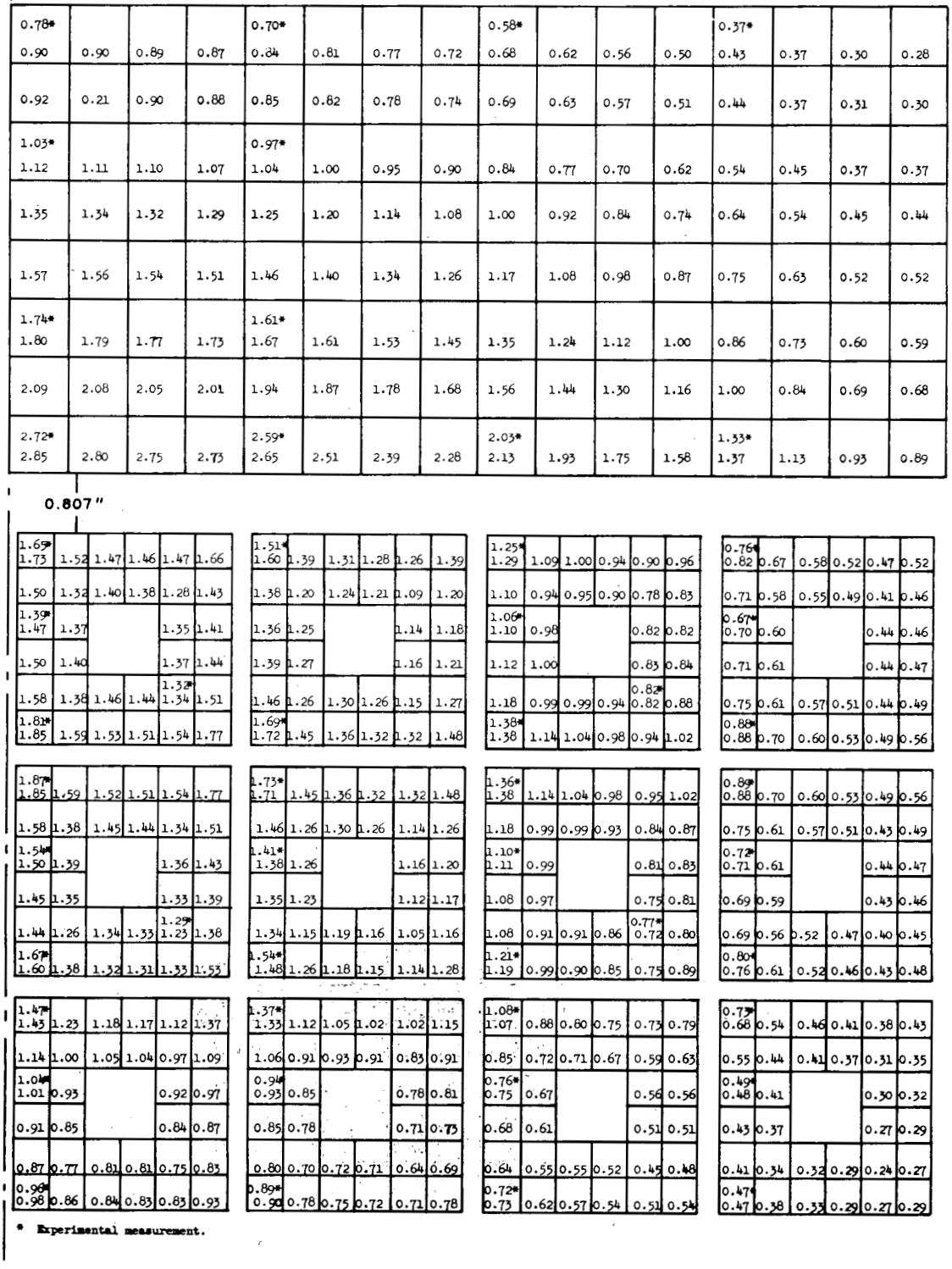

Figure 22. Rod-By-Rod Power Distributions for One-Half of the External Boiler-Superheater Arrangement With Superheater Flooded (Average Rod Power Normalized to Unity)

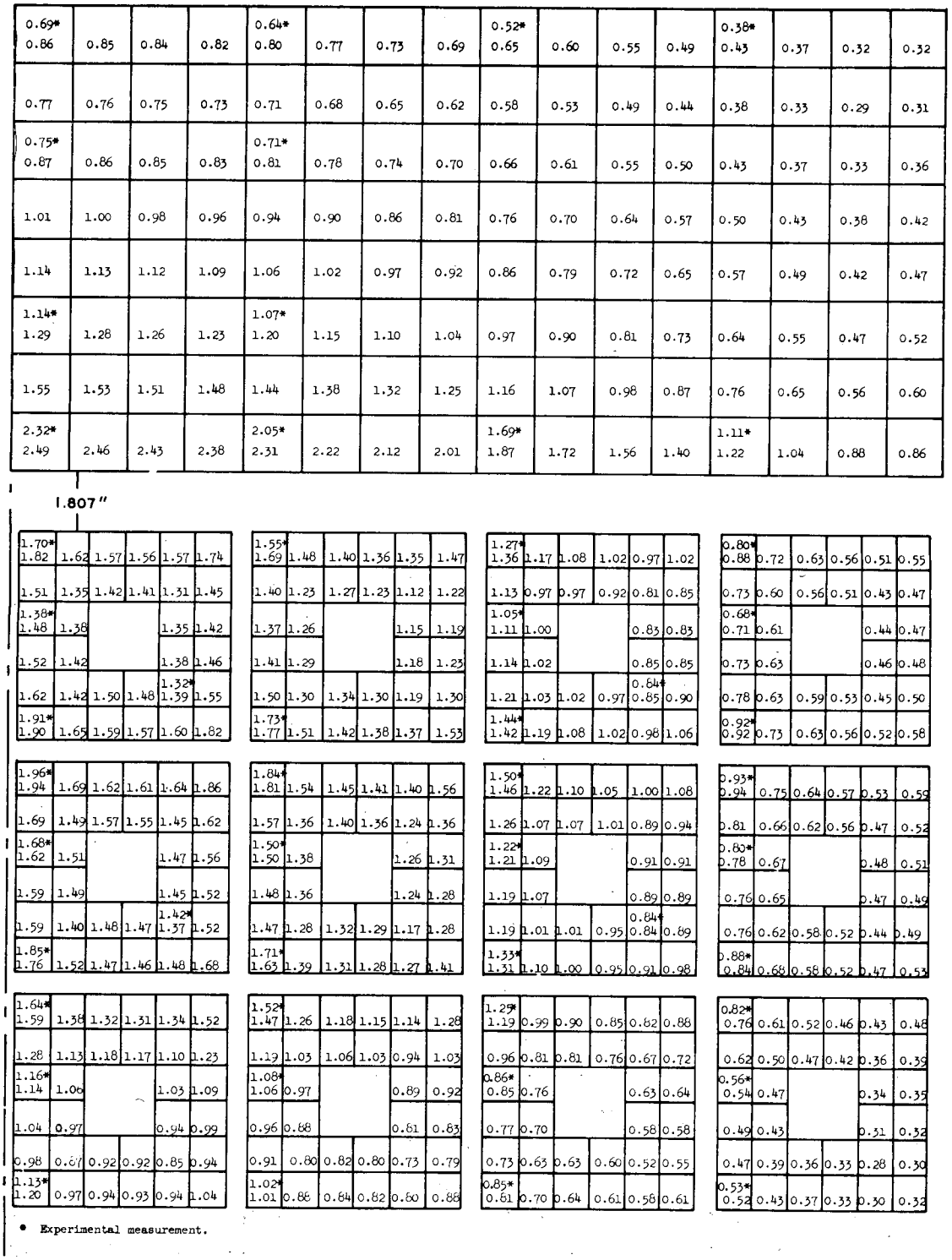

Figure 23. Rod-By-Rod Power Distributions for One-Half of the External Boiler-Superheater Arrangement With Superheater Voided and With Increased Water Channel Between Boiler and Superheater Region (Average Rod Power Normalized to Unity)

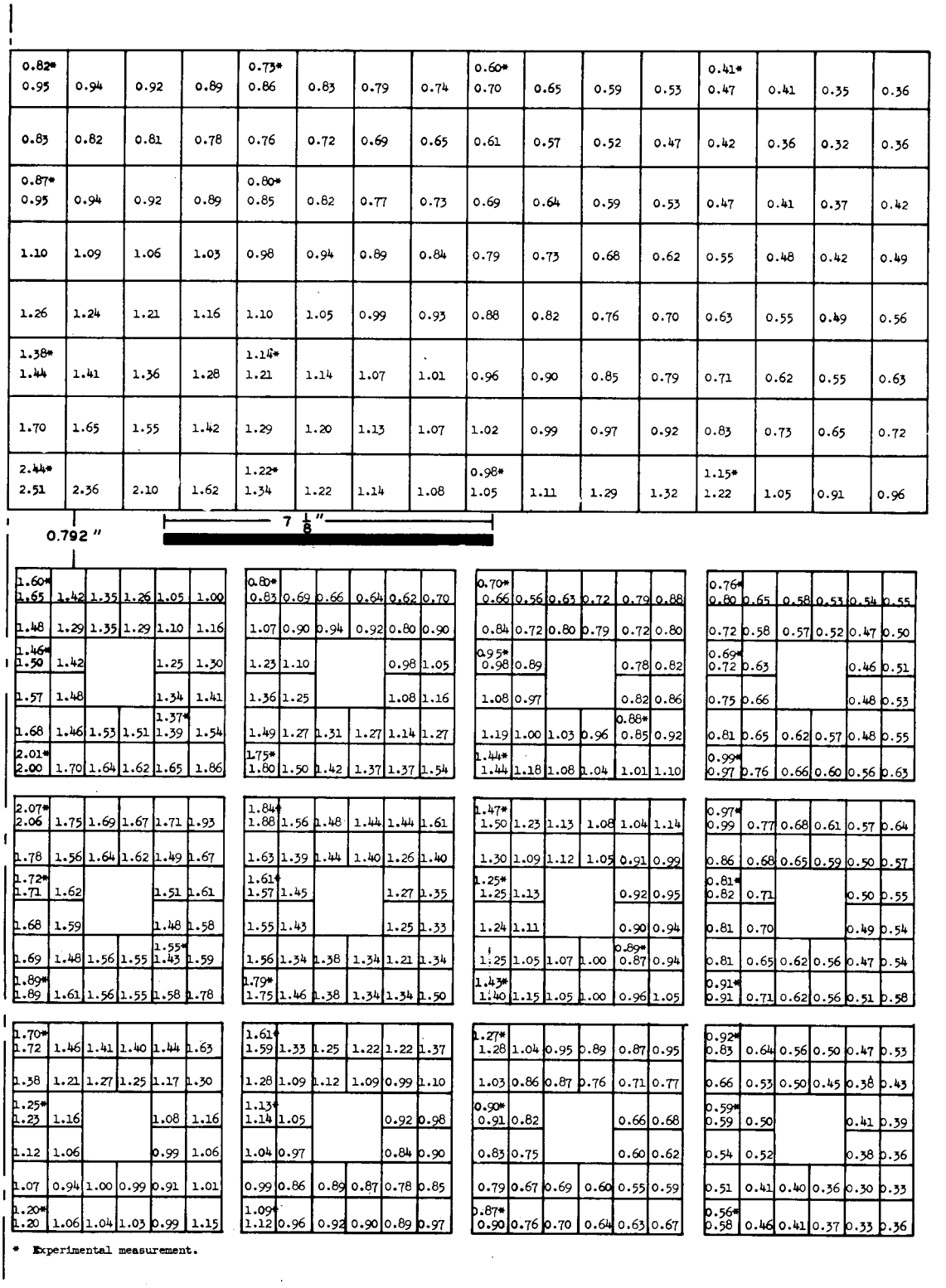

* Experimental measurement.

Figure 24. Rod-By-Rod Power Distributions for One-Half of the External Boiler-Superheater Arrangement With the Superheater Voided and Two 0.131-in. 2.15 wt.% B-SS Control Rods Between Regions. (Average Rod Power Normalized to Unity)